

On the role of trans-lithospheric faults in the long-term seismotectonic segmentation of active margins: a case study in the Andes

Gonzalo Yanez C.¹, Jose Piquer R.², Orlando Rivera H.³

¹ Pontificia Universidad Católica de Chile, Av. Vicuña Mackenna 4860, Macul, Santiago, Chile, gyaneza@uc.cl

² Instituto de Ciencias de la Tierra, Universidad Austral de Chile, jose.piquer@uach.cl

³ Minera Peñoles de Chile, orlando_rivera@penoles.com.mx

Correspondence to: Gonzalo Yanez C. (gyaneza@uc.cl)

Abstract. Plate coupling plays a fundamental role in the way in which seismic energy is released during the seismic cycle. This process includes quasi-instantaneous release during megathrust earthquakes and long-term creep. Both mechanisms can coexist in a given subduction margin, defining a seismotectonic segmentation in which seismically active segments are separated by zones where ruptures stop, classified for simplicity as asperities and barrier, respectively. The spatiotemporal stability of this segmentation has been a matter of debate in the seismological community for decades. At this regard, we explore in this paper the potential role of the interaction between geological heterogeneities in the overriding plate and fluids released from the subducting slab towards the subduction channel. As a case study, we take the convergence between the Nazca and South American plates between 18°-40° S, given its relatively simple convergence style and the availability of a high-quality instrumental and historical record. We postulate that trans-lithospheric faults striking at a high angle with respect to the trench behave as large fluid sinks that create the appropriate conditions for the development of barriers and promote the growth of highly coupled asperity domains in their periphery. We tested this hypothesis against key short- and long-term observations in the study area, seismological, geodetic, and geological, obtaining consistent results. If the spatial distribution of asperities is controlled by the geology of the overriding plate, seismic risk assessment could be established with better confidence.

1 Introduction

Subduction margins accommodate short-term (years to tens of years) and long-term (thousands to millions of years) deformation. The most evident effects of these two deformational behaviours are earthquakes (short-term) and mountain-building (long-term) (e.g. Avouac, 2007). The concept of the seismic cycle, introduced by Fedotov (1968) and further elaborated by Mogi (1977, 1985), identifies two stages: a long inter-seismic period

34 (several tens of years), followed by a short co-seismic period (minutes at most) where the elastic energy stored
35 during the previous stage is released as an earthquake. For earthquake magnitudes in the range of M_w 7.5–9.5,
36 the observed mean slip displacement varies from 0.8–10 meters (Thingbaijam et al., 2017). Even though the
37 maximum mean slip in megathrust events is 10 meters, the zones of maximum slip, equated to asperities (e.g.,
38 Aki, 1984, Lay & Bileck 2007, Lay 2015) can reach 20–40 meters in wavelength patches in the range of 20–
39 100 kilometres (see, e.g., <http://equake-rc.info/srcmod/>). However, the release of elastic energy during the
40 seismic cycle only accounts for 90–95% of the deformation accumulated interseismically in convergent margins;
41 the remaining 5–10% produces permanent deformation in the overriding plate, expressed as crustal shortening
42 and mountain building (e.g. Yañez and Cembrano, 2004). This long-term process lasts for hundreds to
43 thousands of seismic cycles (time windows of millions of years). Therefore, both phenomena — earthquakes
44 and mountain building — are extreme responses to the same process: the convergence between oceanic and
45 continental plates.

46 The concepts of asperities and barriers were proposed by Lay et al. (1982) and Aki (1984) to describe the
47 process during the occurrence of an earthquake and intimately related to the concept of plate coupling. More
48 recent studies (e.g. Bileck and Lay, 2007) propose a more complex mechanism at the subduction plate contact,
49 in which domains of unstable stick-slip state coexist with other domains in a conditionally stable stick-slip state,
50 and zones that develop aseismic slip/stable behaviour. These three states — unstable, conditionally stable, and
51 stable stick-slip behaviour — represent different slip modes that can be represented as asperities and barriers in
52 the old nomenclature (Scholz, 1990). However, the conceptualization of Bileck and Lay (2007) proposes an
53 down-dip (depth) distribution of the different slip behaviours: (1) aseismic-stable at depths of 5–10 kilometres,
54 (2) mostly conditionally stable at depths of 10–15 kilometres, and (3) unstable stick-slip behaviour (Brace and
55 Byerlee (1966) and Burridge and Knopoff (1967)) at depths of 15–25 kilometres. Recent studies on exhumed
56 subduction domains in California (Platt et al., 2018) corroborate this down-dip transition from seismic zone to
57 transition zone. One interesting characteristic of these domains is that unstable domains are generally
58 surrounded by conditionally stable domains and aseismic domains in their outermost periphery.

59 To date, there is no clear evidence on whether the geological/tectonic process(es) control to some extent these
60 seismogenic behaviours and/or their stability across several seismic cycles or geological time frames. Potential
61 candidates already proposed include: (1) the roughness of the subducting plate (aseismic ridges, fracture zones,
62 horst/graben structures, etc.) (e.g. Bilek et al., 2003, Wang and Bilek, 2011; Gersen et al., 2015; Philibosian and
63 Meltzner, 2020; Molina et al., 2021); (2) fluid-controlled overpressure (Peacock, 1990; Safer and Tobin, 2011;
64 Safer, 2017; Menant et al., 2019); (3) the shape of the subducting plate (e.g. Gutscher et al., 1999); (4) the
65 geology of the overriding plate (i.e Kimura et al., 2018; Philibosian and Meltzner, 2020; Molina et al., 2021),
66 among others, including various combinations of these different possible factors.

67 The role of fluids released from the subducting slab has emerged as a first-order factor in the plate-coupling
68 processes at subduction margins. Direct observations (e.g., Saffer and Tobin, 2011; Tsuji et al., 2014, Moreno
69 et al., 2014) and numerical modelling (Menant et al., 2019) demonstrate that fluids released from the subducting
70 oceanic crust and subduction channel define segments at the plate-coupling zone with distinct pore pressure
71 characteristics. Overpressure domains are associated with zones of weak coupling, and strong coupling is

72 observed in the case of zones showing low pore pressure behaviour. The first type of domain is in direct
73 association with creep zones or slow slip events, while the other one is in direct association with locked zones,
74 or in the seismological nomenclature, the barrier and asperity domains, respectively. Seismic imaging of the
75 forearc wedge (e.g. Tsuji et al., 2014) and numerical modelling also show that fluids percolate upwards in the
76 zones of maximum overpressure, including the emplacement of serpentinite bodies along weak zones or faults.

77
78 In this paper, we propose a causal relationship between the presence of trans-lithospheric faults (TLF) in the
79 overriding plate and seismic segmentation, involving the control of TLF on the movement/storage/release of
80 overpressure fluids along and across the subduction zone. We use the Central Southern Andes as a case study,
81 as it is one of the most active seismogenic sites worldwide, is well studied, and has a relatively simple
82 subduction geometry (Hayes, 2018). In addition, recent structural and geophysical mapping has revealed the
83 role of TLF in the tectono-magmatic evolution of the continental margin of this region (e.g. Yáñez et al., 1988,
84 Santibáñez et al., 2019; Cembrano and Lara, 2009; Melnick and Echtler, 2006; Yáñez and Rivera, 2019; Piquer
85 at al., 2019, 2021a). We aim to demonstrate that the interaction between these TLF and the fluid circulating
86 through the subduction channel provides a simple first-order explanation for the Andean seismotectonic
87 organization through a long-lived geological control.

88 **2 Data and methods**

89 **2.1 Tectonic background**

90 The Nazca-South American plate convergence is a subduction-type margin that has been active in this segment
91 of the Andes since at least the Cretaceous without the accretion of new terrains (Mpodozis and Ramos, 1990).
92 Since 15 Ma, the convergence has been slightly oblique (E10°N) at a velocity of around 6.5 cm/yr (Angermann
93 et al., 1999). The age of the oceanic plate varies between 0 Ma at the triple junction of Taitao (44°S) to 45 Ma
94 at the Orocline bending of Bolivia (18°S) (Figure 1). A flat slab segment is located between 28°S and 33°S
95 latitude, affecting the development of an asthenospheric wedge landward and inhibiting the occurrence of active
96 volcanism since the last 5 Ma (Kay and Mpodozis, 2002). However, the Wadati-Benioff plane is roughly
97 homogenous in dip along the plate boundary between the Nazca and South American plates (Slab 2.0, Hayes,
98 2018). The roughness of the Nazca plate is affected by a progressively older oceanic crust northward, with some
99 fracture zones offsetting the plate, the subduction of a triple junction with an active spreading centre (now at
100 Taitao Peninsula), some episodic magmatic activity along the Juan Fernandez Ridge (33°S, Yáñez et al., 2001),
101 and eventually a smaller ridge at 20°S (Perdida Ridge, Cahill and Isacks, 1992). Overall, these features can be
102 described as minor obstacles to the subduction of a relatively young oceanic plate underneath a continental plate
103 in a highly coupled convergent margin (Section 2.5).

104

105 **2.2 Compilation of trans-lithospheric faults in the Andean active margin and their role as long-lived** 106 **high-permeability domains**

107 Trans-lithospheric faults (TLF) correspond to long-lived, high-angle fault systems, which have been identified
108 in several segments of the Andean margin, based on geological mapping (e.g. Santibañez et al. 2019; Cembrano
109 and Lara, 2009; Melnick and Echtler, 2006; Piquer et al., 2021a; Farrar et al., 2023; Wiemer et al., 2023), crustal
110 seismicity (e.g. Talwani, 2014.), a combination of indirect geophysical techniques (Yañez et al., 1998), or a
111 combination of all of these (Yañez and Rivera, 2019; Piquer et al., 2019; Pearce et al., 2020). The geometry and
112 depth extension of TLF is unknown, but based on their control of the continental-scale magmatic and
113 hydrothermal processes and their surface traces in the order of hundreds of kms, we consider that they involve,
114 exclusively, the whole lithosphere.

115 In Table 1 we present a synthesis of the current status of knowledge regarding TLF definition and the major
116 geological/geophysical evidences that described them. The number assigned in each case is used later on in
117 Figure 1 as an identificatory.

118 Detailed structural mapping in various segments of the Andean margin has provided direct geological evidence
119 for the presence of TLF. They are manifested in the field as networks of individual high-angle faults, defining
120 deformation zones with widths of up to several kilometres, and lengths in the order of hundreds of kilometres,
121 being possible to follow their trace across the entire continental margin (Lanza et al., 2013; Yañez and Rivera,
122 2019; Piquer et al., 2021a). These fault networks correspond to the expression at the present-day surface of a
123 pre-existing TLF, as a result of its vertical propagation through Mesozoic and Cenozoic igneous and
124 sedimentary rocks (McCuaig and Hronsky, 2014; Piquer et al., 2019). Field observations also show that,
125 consistent with their high dip angle (commonly $>60^\circ$ and in several cases sub-vertical, although individual fault
126 segments can dip at slightly lower angles), TLF tend to be reactivated as basin-bounding faults during
127 extensional episodes, and are thus associated with sharp changes in the stratigraphic record (Piquer et al., 2015,
128 2021a; Yañez and Rivera, 2019). They also control the distribution of exhumed basement blocks (Yañez and
129 Rivera, 2019).

130 The geological record demonstrates that TLF are long-lived structures, that have played a major role in the
131 long-term evolution of the Chilean continental margin, being reactivated with different kinematics under
132 varying tectonic regimes. It is likely that several TLF were originated in the Proterozoic and the Palaeozoic
133 (Yañez and Rivera, 2019); there is strong geological evidence suggesting the present-day TLF architecture was
134 already in place by the Permo-Triassic, a period in which these structures acted as master and transfer faults for
135 intra-continental rift systems (Niemeyer et al., 2004; Sagripanti et al., 2014; Espinoza et al., 2019). Syn-tectonic
136 emplacement of magma along TLF has been documented at least since the Jurassic (Creixell et al., 2011).

137 Geophysical support for the TLF architecture in the continental margin is provided by the geometry of magnetic
138 and gravimetric anomalies (Piquer et al., 2019; Yañez and Rivera, 2019) and also by magnetotelluric data
139 (Pearce et al., 2020) and seismic tomography (Yañez and Rivera, 2019). Evidence of seismic activity in some
140 of these TLF has been recorded, for example, a precursory event to the 9.3 Mw 1960 Valdivia Earthquake
141 (Lanahue fault, Melnick et al., 2009), and the coseismic rebound associated with the 8.8 Mw 2010 Maule
142 earthquake (Pichilemu fault, e.g. Farías et al, 2011; Aron et al., 2013). Additionally, researchers have
143 documented a strong spatial relationship between a TLF and a major seismic swarm (Valparaíso seismic
144 sequence of 2017, Nealy et al., 2017) at the subduction megathrust (Piquer et al., 2021a).

145 Regarding the role of TLF as long-lived high-permeability domains, Yañez and Rivera (2019) postulated that
146 they represent weak lithospheric domains that favour fluid flow and the emplacement of different types of ore
147 deposits over large time periods (tens of millions of years), beginning with stratabound and IOCG-type deposits
148 in the Jurassic. A similar conclusion has been reached by Farrar et al. (2023) for the emplacement of porphyry
149 copper deposits of various ages, and by Wiemer et al. (2023) for gold-rich superclusters of various types of
150 mineral deposits. The strong relationship between the locations of TLF and those of giant ore deposits at specific
151 metallogenic belts has been discussed more specifically in the Andes of Northern (e.g., Chernicoff et al., 2002)
152 and Central Chile (e.g., Piquer et al., 2016) and neighbouring regions in Argentina. Similarly, there is a well-
153 established relationship between the locations of TLF and volcanic/geothermal activity in the Andes of Southern
154 Chile (e.g., Cembrano and Lara, 2009). Moreover, high Vp/Vs ratios that were documented during the
155 Pichilemu seismic sequence following the 2010 Maule earthquake have been interpreted as strong evidence of
156 fluid migration (Fariás et al., 2011, Calle-Gardella et al., 2021).

157 Various authors have discussed how the type of magmatic-hydrothermal product and fluid flow regime varies
158 depending on the orientation of a specific high-angle fault system (in several cases, a TLF) relative to the
159 predominant stress tensor (Lara et al., 2006; Cembrano and Lara, 2009; Roquer et al., 2017; Piquer et al.,
160 2021b). Of particular relevance is the orientation of the fault system relative to the maximum stress (σ_1); if the
161 fault system is sub-parallel or strikes at a low angle relative to σ_1 , it is well-oriented for opening and reactivation
162 respectively, allowing the rapid ascent of magma and hydrothermal fluids through different crustal segments.
163 On the other hand, if the fault system is sub-perpendicular or strikes at a high angle relative to σ_1 , it would be
164 poorly oriented or misoriented for reactivation and would promote the storage of magma and hydrothermal
165 fluids at depth (e.g. Cembrano and Lara, 2009; Stanton-Yonge et al., 2016; Piquer et al., 2021b). In the latter
166 case, a requirement for fault reactivation and the release of the accumulated fluids is that supra-lithostatic fluid
167 pressures are achieved; once this occurs, the fault system would allow the discharge of the accumulated fluids
168 towards upper crustal levels and would act as a fluid pump (“fault-valve behaviour”), concentrating fluids in
169 the fractured areas within the fault system and leading to the depletion of fluids in the surrounding regions
170 (Sibson, 1990, 2020; Cox, 2016). These fluid discharge events cause seismic swarms (Cox, 2016), which
171 concentrate at the base of the high-angle fault system (Sibson, 2020).

172 Figure 1 presents the main array of NW- and NE-striking TLF observed in the Andean margin; their seaward
173 trend has been extrapolated following the observed trend in the continental lithosphere, in particular south of
174 36°S, following the trace of submarine canyons.

175

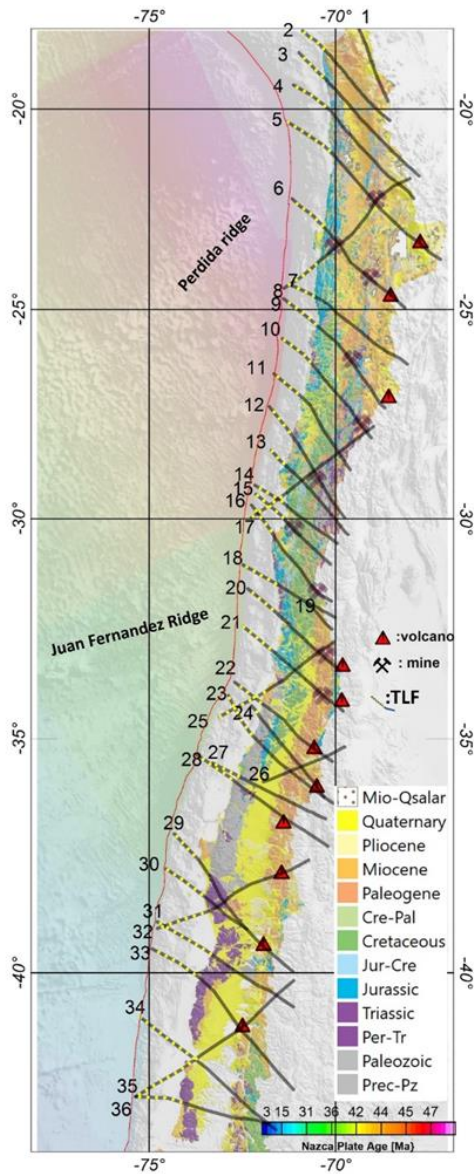
Table 1: Main Trans-Lithospheric Faults of the Chilean Andes (17-42°S Latitude)

LSS_ID	LSS_NAME	REFERENCES	GEOLOGICAL EVIDENCES
1	Visviri	(15), (22)	(L)(TLS)(SC)(GVA), Antofalla Basement (T)
2	Arica	(15), (21), (22)	Arequipa Massif (T), ETL NW Arica (TLS)
3	Camarones	(22)	(TLS)(GVA)(SDGU)
4	Iquique	(22)	(TLS)(GVA)(SDGU)
5	Calama	(1), (2), (8), (20), (21), (22), (24)	Comache (F), Calama-Olapato-El Toro (L)(FS)(VA), Solá (F), Chorrillos (F), ETL NW Calama (TLS)
6	Mejillones-Llullaillaco	(8), (10), (21), (22), (29), (35)	Archibarca (L)(VA), Cataclasis de Sierra de Varas (DZ), ETL NW Mejillones (TLS), Socompa (FS)
7	Agua Verde-Exploradora	(8), (22)	Culampajá (L)
8	Antofagasta-Conchi	(22), (27), (28), (30)	Antofagasta-Calama (L)(PMG)(TR)(STMH)
9	Taltal-Potrerrillos	(8), (22)	Taltal (L)(TLS)(SDGU)(VA)(STMH)
10	Chañaral	(8), (22)	(TLS)(GVA)(SDGU)
11	Copiapó	(22)	(TLS)(SDGU)
12	Vallenar	(22)	(TLS)(SDGU)
13	Domeyko	(22), (36)	(TLS)(GVA)(SDGU), Cruzadero (F)
14	Vicuña	(22)	(TLS)(GVA)(SDGU)
15	Andacollo	(22)	(TLS)(GVA)(SDGU)(STMH)
16	Punitaqui-Los Pelambres	(22)	(TLS)(GVA)(SDGU)(MA)(STMH)
17	El Potro	(22)	(TLS)(SDGU)
18	Illapel	(22)	(TLS)(GVA)(SDGU)
19	Almendrillo	(22)	(TLS)(GVA)(SDGU)
20	La Ligua-Los Andes	(21), (22), (31)	(TLS)(GVA)(SDGU)(SC)(MA), Río Blanco-Los Bronces (FS)(STMH)
21	Valparaíso-Volcán Maipo	(3), (5), (7), (19), (21), (22), (23), (26)	Piuquencillo (F)(FS)(STMH), Melipilla (F)(MA), Marga-Marga (FS), Valparaíso-Curacaví (FS)(STMH), Concón (MDS), Cartagena (MDS), El Tabo (MDS)
22	Pichilemu	(9), (17), (22), (23), (24), (25)	Pichilemu (ATS), Teno (FS)(SC)(STMH), Planchón-Peteroa (LLBS)(SC)
23	Laguna del Maule	(32), (33)	Río Maule (F)(VA)(SDGU)(STMH)
24	Iloca-Río Melado	(34)	Laguna Fea (FS)(VA)(STMH)
25	Aconcagua-San Antonio	(4), (6), (22), (23), (31)	Puangue (F), Estero Chacabuco (F), Estero Colina (F), El Salto (FS)(STMH)
26	Volcán Quizapu	(33)	(VA)(MDS)
27	Parral-Bullileo	This study	(VA)(SDGU)
28	San Carlos-Nevados de Chillán	(12), (17), (18)	Chillán (AZ), Nevados de Chillán-Tromen (LLBS), Cortaderas (L)
29	Lanahue-Volcán Villarrica	(11), (14), (16), (17), (24)	Morguilla (FLS), Lanahue (F)(FS), Villarrica-Quetrupillán-Lanín (LLBS)
30	Tirúa-Pitrufquén	(11), (16)	Mocha-Villarrica (FS)
31	Río Calle Calle-Lago Ranco	(13), (17)	Carrán-Los Venados (LLBS), Futrono (F)
32	Puerto Saavedra-Volcán Callaqui	(18)	Copahue-Callaqui (AZ)
33	Osorno-Volcán Calbuco	This study	(VA)
34	Ancud-Volcán Michimahuida	(17)	Michimahuida (LLBS)
35	Cucao-Chaitén	(17)	Chaitén (LLBS)
36	Chacao-Osorno-Puntiagudo	(17)	(VA)

Abbreviations: (ATS) Andean Transverse System; (AZ) Accommodation Zone; (DZ) Deformation Zone; (F) Fault; (FLS) Fault-line Scarp; (FS) Fault System; (GVA) Gravimetric Anomaly; (L) Lineament; (LLBS) Long-Lived Basement Structures; (LLTF) Long-Lived Transverse Fault; (MA) Magnetic Anomaly; (MDS) Mafic Dike Swarm; (PMG) Paleomagnetism; (SC) Seismic Cluster; (SDGU) Structural Discontinuity of Geological Units; (T) Terrane; (TLS) Translithospheric Structures; (TR) Tectonic Rotations; (STMH) Syn-Tectonic Magmatic-Hydrothermal Centers; (VA) Volcano Alignment.
Reference Keys: (1) Salfity, 1985; (2) Marrett et al., 1994; (3) Gana et al., 1996; (4) Wall et al., 1996; (5) Yáñez et al., 1998; (6) Wall et al., 1999; (7) Rivera & Cembrano, 2000; (8) Chernicoff et al., 2002; (9) Sernageomin, 2003; (10) Niemeyer et al., 2004; (11) Haberland et al., 2006; (12) Ramos & Kay, 2006; (13) Lara et al., 2006; (14) Glodny et al., 2008; (15) Ramos, 2008; (16) Melnick et al., 2009; (17) Cembrano & Lara, 2009; (18) Radic, 2010; (19) Creixell et al., 2011; (20) Lanza et al., 2013; (21) Rivera, 2017; (22) Yáñez & Rivera, 2019; (23) Piquer et al., 2019; (24) Santibáñez et al., 2019; (25) Pearce et al., 2020; (26) Piquer et al., 2021a; (27) Arriagada et al., 2003; (28) Peña, 2010; (29) Richards et al., 2013; (30) Palacios et al., 2007; (31) Piquer et al., 2015; (32) Kohler, 2016; (33) Fischer, 2021; (34) Torres, 2021; (35) Farrar et al., 2023; (36) Giambiagi et al., 2017.

179

180



181

182 **Figure 1: The spatial distribution of trans-lithospheric faults (TLF) over the regional geology of the Chilean**
183 **continental margin (from SERNAGEOMIN, 2003). The traces of the TLF's are based on the models of Yáñez and**
184 **Rivera (2019) and Piquer et al. (2019) in Northern and Central Chile, and after the model of Melnick and Echtler**
185 **(2006) in Southern Chile. Also shown are the locations of the main ore deposits (from north to south, Chuquicamata,**
186 **Mantos Blancos, Escondida, Salvador, Cerro Casale, El Indio, Andacollo, Los Pelambres, Río Blanco-Los Bronces**
187 **and El Teniente), and active volcanoes (from north to south, Lásca, Llullaillaco, Ojos del Salado, Tupungatito,**
188 **Maipo, Planchón-Peteroa, Laguna del Maule, Chillán, Callaqui, Villarrica and Osorno) to show their**
189 **correspondence with the TLF array. TLF are extended until the trench, following their main trend and the canyons**
190 **trace to the south of 36°S, using segmented red lines to highlight the uncertainty of this offshore extension. In the**
191 **seaward side of the figure, the age map of Müller et al. (2019) is included with the bathymetry of the seafloor.**

192

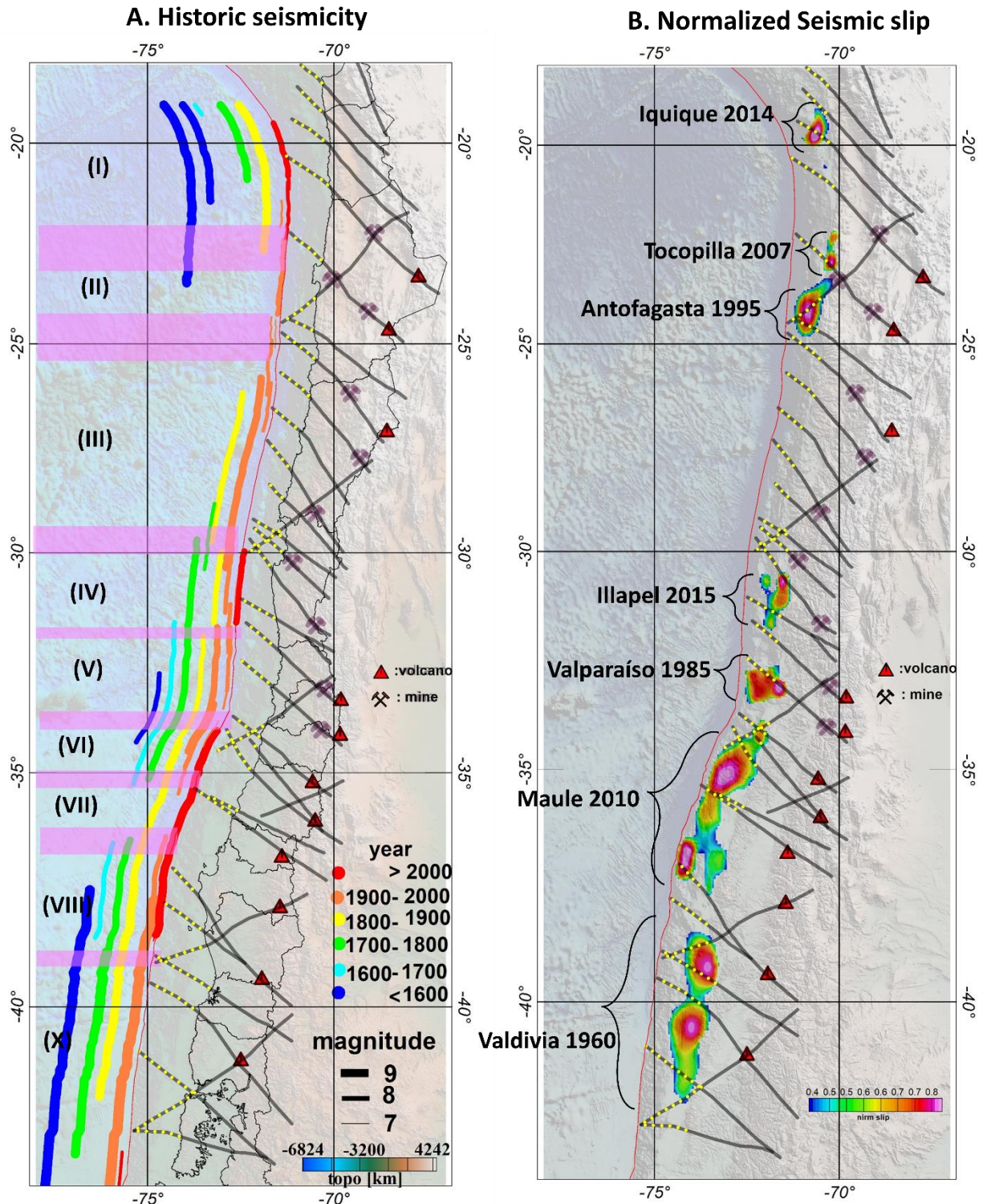
193 **2.3 Historic subduction seismicity and Slip solutions during the last 50 years and Trans-lithospheric**
194 **faults (TLF) correspondance**

195 The historic seismic record in the region is short, extending from the start of the Spanish Colonization in the
196 region (present territories of Perú and Chile, circa 1500 ac). Compilations of historic seismicity and subsequent
197 interpretation to assess the magnitude and longitudinal extension of the events have been provided in Ruiz and
198 Madariaga (2018) and Scholz and Campos (2012), among others. Figure 2, panel A, includes all the historic
199 events described by these authors, as well as events above 7 Mw from the USGS catalogue. As noted by several
200 authors (Ruiz and Madariaga, 2018, and references therein), there is evidence of seismo-tectonic segmentation
201 in the historic record. For the present analysis, we define seven domains from north to south; the boundary
202 between domains is defined by a region of roughly 100-200 kilometres that represents the uncertainty in the
203 rupture length of the major events. We consider wider boundaries for the cases of lacking information, in
204 particular in the northern area where the historic record is scarce. Domain I, in the northernmost part of the
205 study region, shows a sequence of events close to magnitude 8 Mw and separated by 100–150 years. Domain
206 II has no large events (above 8 Mw) in the historic record, instead having a series of intermediate events of
207 magnitude 7–7.7 Mw between 1960 and 2020. Domain III has two events with magnitudes in the range 8.3–8.5
208 Mw separated by almost 10 years, but with a current seismic gap of 100 years. Domain IV is less than 200
209 kilometres in length and includes a series of seismic events of magnitude 8 Mw or above. According to Ruiz
210 and Madariaga (2018), the three major events in this domain show relatively consistent recurrence times (60–
211 80 years) and magnitudes (8–8.4 Mw), namely, the earthquakes of 2015 (Illapel, 8.3 Mw), 1943, and 1880.
212 Domain V is also relatively small, about 300 km, and includes regular events of around magnitude 8 Mw,
213 including the Valparaiso 1985 8 Mw event and the 1906 8.4 Mw event. Domain VI, VII and VIII include part
214 of the Maule 2010 8.8 Mw and Concepción 1835 8.6 Mw events, but are defined as such based on some less
215 than 8 Mw events, Domain X, the southernmost domain, is dominated by the giant events of Valdivia 1960, 9.5
216 Mw, and 1737, 9.0 Mw.

217 Adequate seismic coverage is available since 1985 in Chile. In this period, six large earthquakes have been
218 recorded: Valparaiso 1985, 8.0 Mw (Comte et al., 1986; Mendoza et al., 1994); Antofagasta 1995, 8.0 Mw
219 (Ruegg et al.; 1996, Delouis et al., 1997; Pritchard et al., 2002 and Chlieh et al., 2004); Tocopilla 2007, 7.8 Mw
220 (Schurr et al., 2012); Maule 2010, 8.8 Mw (Delouis et al., 2010; Lay et al., 2010; Vigny et al., 2011; Koper et
221 al., 2012; Ruiz et al., 2012; Moreno et al., 2012; Lorito et al., 2011; Lin et al., 2013; Yue et al., 2014); Iquique
222 2014, 8.2 Mw (Ruiz et al., 2014; Hayes et al., 2014; Schurr et al., 2014; Lay et al., 2014), and Illapel 2015, 8.3
223 Mw (Melgar et al., 2016; Heidarzadeh et al., 2016; Li et al., 2016; Lee et al., 2016; Satake and Heidarzadeh,
224 2017). Given the large size of the Valdivia 1960 earthquake (9.5 Mw), we also include slip estimates for this
225 event based on surface deformation data (Barrientos and Ward, 1990). The slip distribution of these events
226 ranges from 1 meter (e.g. Tocopilla 2007, Antofagasta 1995), several meters (e.g. Illapel 2015, Iquique 2014),
227 and more than 10 meters (Valdivia 1960, Maule 2010); however, in Figure 2, panel B, we normalize the slip

228 distribution with respect to the corresponding maximum slip in each case, plotting over the slab surface to
229 highlight its spatial distribution. This approach aims to highlight the zones of maximum slip in each case and
230 to appreciate their spatial and temporal distribution, under the working hypothesis that they represent the zones
231 of maximum slip and are most likely a good proxy to identify asperities in the plate contact zone. These
232 maximum slip zones are generally distributed between the TLF network (Figure 2).

233



234
 235
 236
 237
 238
 239
 240
 241

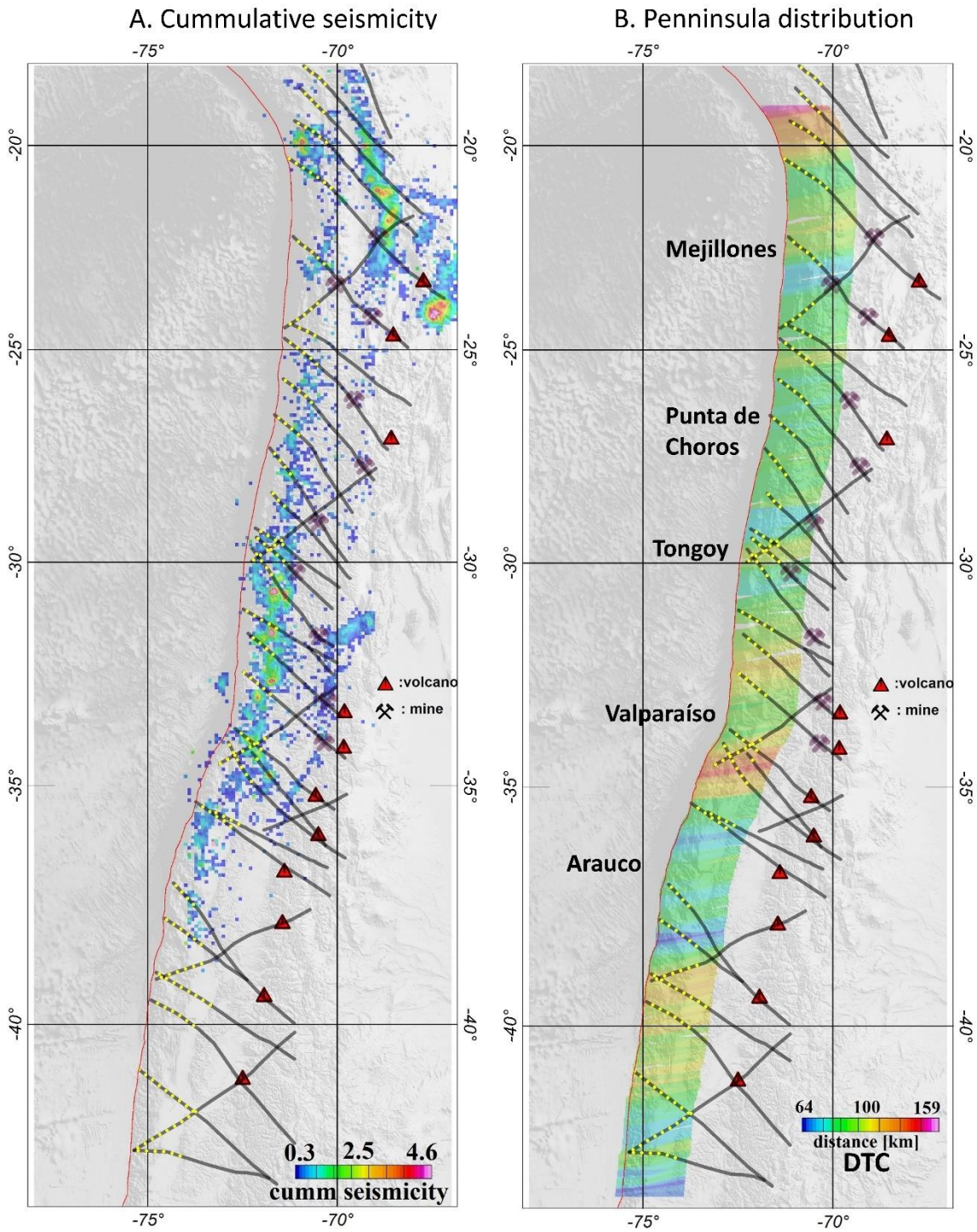
Figure 2: Panel A: historical seismicity from the years 1450 to 2020 (for a full description of each event, see Table A.1 of the supplementary material). The lateral extent of each event indicates the NS estimate of the event name; the colour scale corresponds to the year window of each event; the Mw magnitude is represented by the width of the line. Seismo-tectonic segmentation is indicated by pink semi-transparent ribbons, which are extended downwards to the lower panels. Panel B: zones of maximum slip in the megathrust events registered at the margin of Chile since 1960, colour code represents a normalized slip to the maximum slip in each event.

2.4 Cumulative seismic spatial distribution in the last 20 years

The seismic activity, apart from its spatiotemporal distribution around megathrust events (occasionally with foreshocks and normally with a hyperbolic distribution of aftershocks in time (Omori's law), shows some clustering (denominated in general as seismic swarms), may be triggered by aseismic creep events (Forsyth et al., 2003; Roland and McGuire, 2009) associated with the presence of fluids in the fault zone. In the Andean plate convergence margin, recent studies also show examples of seismic swarm distribution attributable to fluid pore-pressure processes (e.g. Poli et al., 2017, Pasten-Araya et al., 2018). To contextualise the spatial distribution of this seismicity, we compute a normalised seismic density distribution along the margin for the last 20 years in which the seismic network is complete above magnitude 3 Mw. We exclude most of the seismicity associated with major thrust events in this period, filtering out the events at distances of less than 200 kilometres from the rupture zone in a temporal window of 200 days. We acknowledge that this 20-year time window is too short to obtain a broad and complete picture of the distribution of swarms along the margin. However, as swarms normally last for just a few weeks or 1–2 months at most, the cases observed in this time window provide insights into their spatial distribution. The data used in this analysis were obtained from the database of the National Seismological Centre (CNS in Spanish). We selected data attributable to the seismogenic plate contact within a 10-kilometre-thick volume following the slab 2.0 Wadati-Benioff plane (Hayes 2018). The seismic density distribution is shown in Figure 3A, panel A, we can see that seismicity tends to cluster in the vicinity of the seaward projection of the TLF.

2.5 Distance from the trench to the shelf brake

Saillard et al. (2016), show that peninsulas along subduction zones coast lines present a long-term permanent coastal uplift that can be associated with creep and aseismic slip domains. Thus, the distance from the trench to the coast (DTC) constitutes a proxy to separate seismotectonic segmentation due to the weak plate coupling. The physics behind this proposal lies in the dragging force that subduction force induces on the overriding plate, thus with less traction (weak plate coupling in the long term), the fore-arc region close to the trench should be shallower than the surroundings. To gain a broader perspective of the peninsula's distribution, Figure 3B contours the distance to the shelf brake, which is probably a better proxy for a potential uplifted domain in the coastal region. As shown in this figure, the DTC presents variations along the trench. We identify domains of short DTC associated with peninsulas in the region near to: Arauco; Valparaíso; Tongoy; Punta de Choros; and Mejillones. Based on geological and geochronological evidence in three of these peninsulas (Mejillones, Tongoy, and Arauco), Saillard et al. (2016) determined uplift rates in the range of 0.6–2 meters per thousand years in the associated terraces. These terraces have been continuously uplifting for at least the last 0.5–0.8 Myr, indicating a long-term process compared to the seismic cycle of less than 500 years. Using this evidence, in addition to the inter-seismic GPS coupling, Saillard et al. (2016) infer that these peninsula zones are associated with weak plate coupling where deformation is mostly accommodated by creep. Again, qualitatively speaking, there is a tendency to find peninsula distribution where TLF tend to concentrate in the coastal region.



281
 282 **Figure 3: Panel A: density distribution of the last 20 years of seismicity in the margin (data from National**
 283 **Seismological Centre, CSN); values are normalized to better define the zones where seismicity has been**
 284 **concentrated, filtering out all the aftershocks associated with major megathrust activity (Taltal 2001, Maule 2010,**
 285 **Iquique 2014, and Illapel 2015). Panel B: distance from the trench to the shelf brake, projected to the convergence**
 286 **direction (10E).**
 287
 288

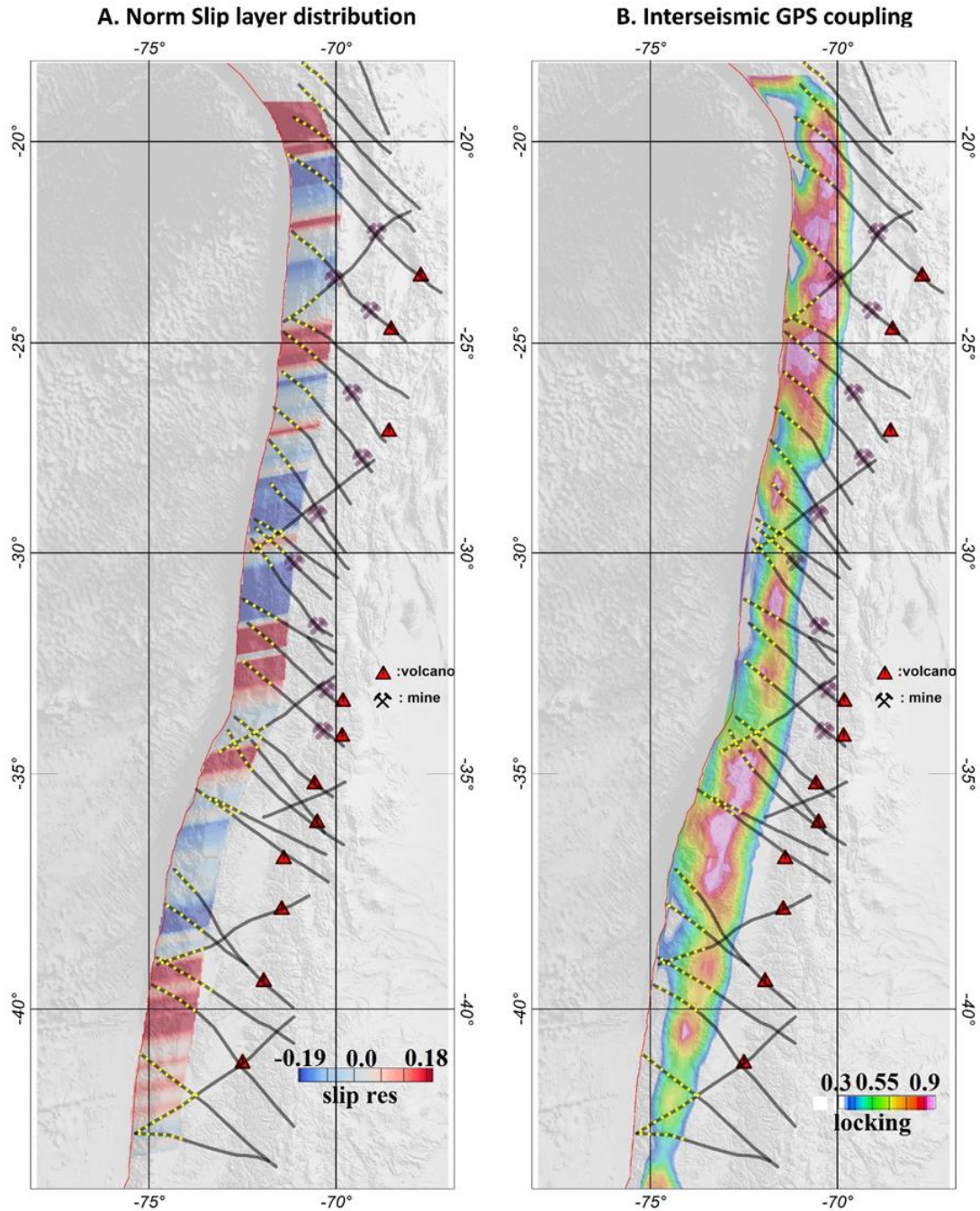
289 **2.6 Viscous coupling**

290 The negative free-air anomaly along the Chile-Perú Trench is the response to dynamic equilibrium between
291 buoyancy and tectonic forces (Yáñez and Cembrano, 2014). The tectonic force tends to drag the continental
292 plate downwards, whereas buoyancy restores this deformation. Assuming equilibrium between the net
293 tectonic force and the long-term deformation (flow in continuum physics) the observed bathymetry represents
294 this force equilibrium. Therefore, for each bathymetric observation, a given Slip Layer Viscosity (SLV)
295 (Wdowinski, 1992) allows a match between observations and long-term viscous plate coupling. Using the
296 methodology developed by Yáñez and Cembrano (2004), we determine the along-strike SLV in the Nazca-
297 South America plate convergence region, considering across-strike profiles every 20 kilometres. As indicated
298 earlier, zones of maximum slip involve wavelengths larger than 20 kilometres for the megathrust events, and
299 therefore, a sample interval of 20 kilometres ensures appropriate along-strike resolution. In addition,
300 following the same rationale and conclusions of Yáñez and Cembrano (2004), we estimate that the increase of
301 the SLV in the north of the study area is due to a temperature-dependent rheology. This increase in viscous
302 plate coupling in the north is likely to be responsible for the larger crustal shortening observed in the southern
303 Andes in the last 20 Ma. Although other authors (e.g. Lamb and Davies 2003) consider that the deficiency in
304 sedimentary supply in the trench in the northern Andes is the driving mechanism for the larger viscous plate
305 coupling in the region. However, this discussion is beyond the scope of the present work, and since the
306 viscous plate coupling correctly represents the observations we are interested here in the short-wavelength
307 viscous plate response as a potential tool to identify zones with different degrees of coupling along the
308 convergent margin. Therefore, we remove this regional viscous plate coupling to isolate short-wavelength
309 features. This residual slip layer viscosity (RSLV) is included in Figure 4A (see a full discussion in
310 Supplement A). This signal shows positive (high relative viscous plate coupling) and negative (weak relative
311 coupling) zones. Again, we use normalized values to highlight the spatial distribution of the signal. In the
312 supplementary material, we present a full description of the modelling used to obtain the RSLV signal. As the
313 modelling is 1D, we extend the result of each model along the strike of the convergence (10°E).

314 **2.7 Inter-seismic GPS coupling**

315 GPS data provide information on the surface deformation relative to a stable continental reference. During the
316 inter-seismic period, the slip velocity at the intraplate contact, Vinter-seismic, can be determined from a GPS
317 network under the assumption of elastic plate deformation (e.g. Okada, 1985). This inter-seismic velocity
318 depends on the degree of plate coupling, ϕ . At maximum plate coupling ($\phi=1$), Vinter-seismic is null, and at
319 minimum plate coupling ($\phi=0$), Vinter-seismic is equal to the convergence velocity ($V_{convergence}$) (e.g.
320 Nuvel1a, De Mets, et al., 1994). Or, mathematically (e.g. Metois et al., 2012), $V_{inter-seismic}=(1-\phi)*$
321 $V_{convergence}$. Inter-seismic GPS coupling is presented as GPS locking data in Panel B of Figure 4 (based in
322 a compilation of GPS information derived from different sources, Burgmann et al., 2005; Chlieh et al., 2008;
323 Loveless & Meade, 2011; McCaffrey et al., 2002; Metois et al., 2012, 2016; Moreno et al., 2010, 2012;
324 Wallace et al., 2004)). For the segment between Antofagasta and Copiapo (24-28°S), two new GPS plate
325 coupling models are available (Yáñez-Cuadra et al., (2022) and González-Vidal et al., (2023)), however, we
326 noticed that these new results share similarities do not depart significantly with the model presented in Figure

327 4b, and is therefore not necessarily thus are not included in this case. From 27°S to the north, high GPS plate
328 coupling is generally observed, although some correspondence is observed with the local minimum and TLF
329 distribution. Between 27°–33°S, the GPS coupling shows domains with lower values with better
330 correspondence with TLF segmentation and the minimum in viscous coupling. To the south of 33°S, the GPS
331 plate coupling shows a spatial distribution that again shows some coincidence with the other proxies, but also
332 some discrepancies. This is not surprising, since GPS inter-seismic plate coupling reflects the quasi-
333 instantaneous coupling of seismo-tectonic segments at different loading stages. Nevertheless, in most of the
334 studied segments, the GPS plate coupling correlates relatively well with the viscous plate coupling, and the
335 location of peninsulas and cumulative seismicity in the last 20 years.
336



337

338 **Figure 4: Panel A: Normalized Residual slip layer viscosity (RSLV) derived from 1D modelling along profiles**
 339 **separated every 10 km and oriented along the Nazca-South American plate convergence (10°N); as this model**
 340 **involves all of the slip layer, its spatial distribution is represented from the trench until 150 km landward, high**
 341 **relative coupling is associated with high residual slip viscosity (see details of this computation in Supplement A) .**
 342 **Panel B: GPS inter-seismic plate coupling, model 2017 (Burgmann et al., 2005; Chlieh et al., 2008; Loveless &**
 343 **Meade, 2011; McCaffrey et al., 2002; Metois et al., 2012, 2016; Moreno et al., 2010, 2012; Wallace et al., 2004).**
 344 **Locking is restricted to the range between 0.3 to 0.9, in order to enhance the relative coupling along the plate**
 345 **coupling zone.**

346 3. Discussion

347 3.1 Quantitative correlation between TLF and plate coupling proxies derived from seismicity 348 distribution, GPS and viscous coupling and coastal morphology.

349 In order to better quantify the correspondence between the spatial distribution of TLF and the indirect estimate
350 of plate coupling described in chapter 3 we present here an objective comparison between them. This task is
351 challenging, taking into consideration the poorly constrained data used: (a) in some cases, regional-scale
352 geological observations (TLF and peninsula distribution); (b) different time-scale coupling estimates (inter
353 seismic GPS locking and long term viscous coupling); (c) poorly resolved GPS solution offshore; (d) 1D
354 modelling of viscous coupling; and (e) The lack of completeness in the seismicity record (historical record of
355 500 years, instrumental record of megathrust events of 50 years, and cumulative seismicity of 20 years)
356 considering a seismic cycle of a couple of hundred years in the margin. Thus, none independent proxy is capable
357 to produce a reliable estimate by itself, but rather a combination of them. Therefore, a thorough analysis is
358 beyond the capabilities of the data source, and what we present here, though quantitative, should be understood
359 as a guide to determine tendencies from different and independent perspectives that as a whole, provide a more
360 robust estimate on the link between TLF and plate coupling in the margin.

361 The approach adopted considered the spatial correlation between TLF and the six proxies described in chapter
362 3, using the Pearson correlation coefficient between two variables (r_{xy}) defined as:

$$363 \quad r_{xy} = \frac{\sum_{i=1}^n (x_i - \bar{x})(y_i - \bar{y})}{\sqrt{\sum_{i=1}^n (x_i - \bar{x})^2 \sum_{i=1}^n (y_i - \bar{y})^2}} \quad (1)$$

365 Where \bar{x} and \bar{y} are the average value of each variable. This function r_{xy} has values between -1 (opposite
366 correlation) to 1 (direct correlation). Values near zero mean weak or null correlation. In the application of the
367 Pearson correlation in this case, the spatial distribution of TLF is always the x_i , and the 6 proxies used in this
368 case are the y_i in each case. A key property of the Pearson correlation coefficient is its invariance to spatial
369 distribution of samples and scale of the two variables. This property is particularly useful in this case where we
370 are trying to correlate very different proxies in terms of spatial distribution and scale. The correlation is
371 performed in moving windows bins of 32x32 km², with an overlap of 50% between correlation estimates. The
372 correlation is calculated in a domain of 140 km width from the trench to the east, the plate coupling zone where
373 short-term and long-term processes take place.

374 TLF are defined as line traces, but in order to spatially correlate them with the other variables, we add
375 a width, considering potential spatial uncertainties and zones of influence. Thus, the width of each TLF is treated
376 as a gaussian with a value of 1 in the centre and 0 at the edge, located at 10 km from the centre, representing
377 the deformation zone and the lateral surface covered by the potential fluid release. Such a width of 20 km seems
378 a reasonable number for a fault system of more than 100 km length (>20%). In fact, in recorded earthquakes,
379 like the Landers earthquake 1992 (Mw 7.3) where a rupture length of 85 km has been determined the shear
380 deformation zone reached 12-16 km (Perrin et al., 2020). Outside the TLF domains a value of -1 indicates no
381 spatial distribution of TLF, but in practice is not relevant because the correlation is focussed inside the TLF

382 domain only. The other six proxies are treated in a different manner, depending on their nature. GPS plate
383 coupling is a spatial variable covering the whole spatial range of the coupling. Looking at the GPS coupling
384 described in Figure 4b, we can see that most of the plate contact is highly coupled, well above 0.6 almost
385 everywhere, thus in order to identify some differences in coupling we setup the mean value at 0.8. Slip viscosity
386 layer and distance from the shelf brake to the trench are single values varying with latitude that are extended to
387 spatial variables projecting the value landward following the convergence direction ($\sim 10^\circ\text{E}$). In the case of the
388 slip coupling a mean value is already removed, thus a mean value of 0 is considered. For the shelf brake-trench
389 distance we use the average separation of 100 km as the mean value. Seismic cumulative density and slip
390 distribution of megathrust events define restrictive domains along the plate coupling region. These areas are
391 normalized between 1 and zero, and outside the region a value of -1 is assigned (no data). The same procedure
392 is used for the boundary between historic seismicity segmentation, value 1 in the transition, and -1 outside.
393 Since the analysis is restricted to the correlation between TLF's and the six proxies, the correlation only
394 concerns the inner part of the TLF. Given the nature of each proxy, a low coupling at a given TLF implies a
395 negative Pearson correlation at GPS and viscous coupling, distance from the shelf brake to the trench, and slip
396 distribution for megathrust events (maximum slip should lie outside the TLF domain). On the contrary, positive
397 Pearson correlation is expected with the historic segmentation and cumulative seismicity, to reflect low coupling
398 at the TLF domain.

399 The results for each Pearson correlation coefficient spatial distribution are presented in Figure 5 in a
400 plan view. In Figure 8 we present the result for the 32 relevant TLF in terms of the histogram obtained for the
401 Pearson correlation inside the corresponding TLF domain. Over the histograms observations we include an
402 interpretation on the correspondence with a low plate coupling condition, depending on the shape of the
403 histogram, positive (Pearson correlation biased to the left in GPS, VISC, DIST, SLIP histograms; and biased to
404 the right in the CUMM and HIS histograms), unclear (flat for all the proxies) and negative (Pearson correlation
405 biased to the right in GPS, VISC, DIST, SLIP histograms; and biased to the left in the CUMM and HIS
406 histograms) correlation. Based on this analysis we qualify the potential of each TLF in terms of its barrier
407 potential, high, ambiguous, and poor. The criteria to establish this qualification considers the following: (a) high
408 potential: at most one correlation is negative and by majority are positive correlation; (b) ambiguous: at most
409 two correlations are negative and at least one correlation is positive; (c) poor: when more than three correlations
410 are negative or none of them are positive.

411 Some relevant conclusions arise from the spatial analysis of Figure 5, 6 and 7, and histograms of Figure
412 8:

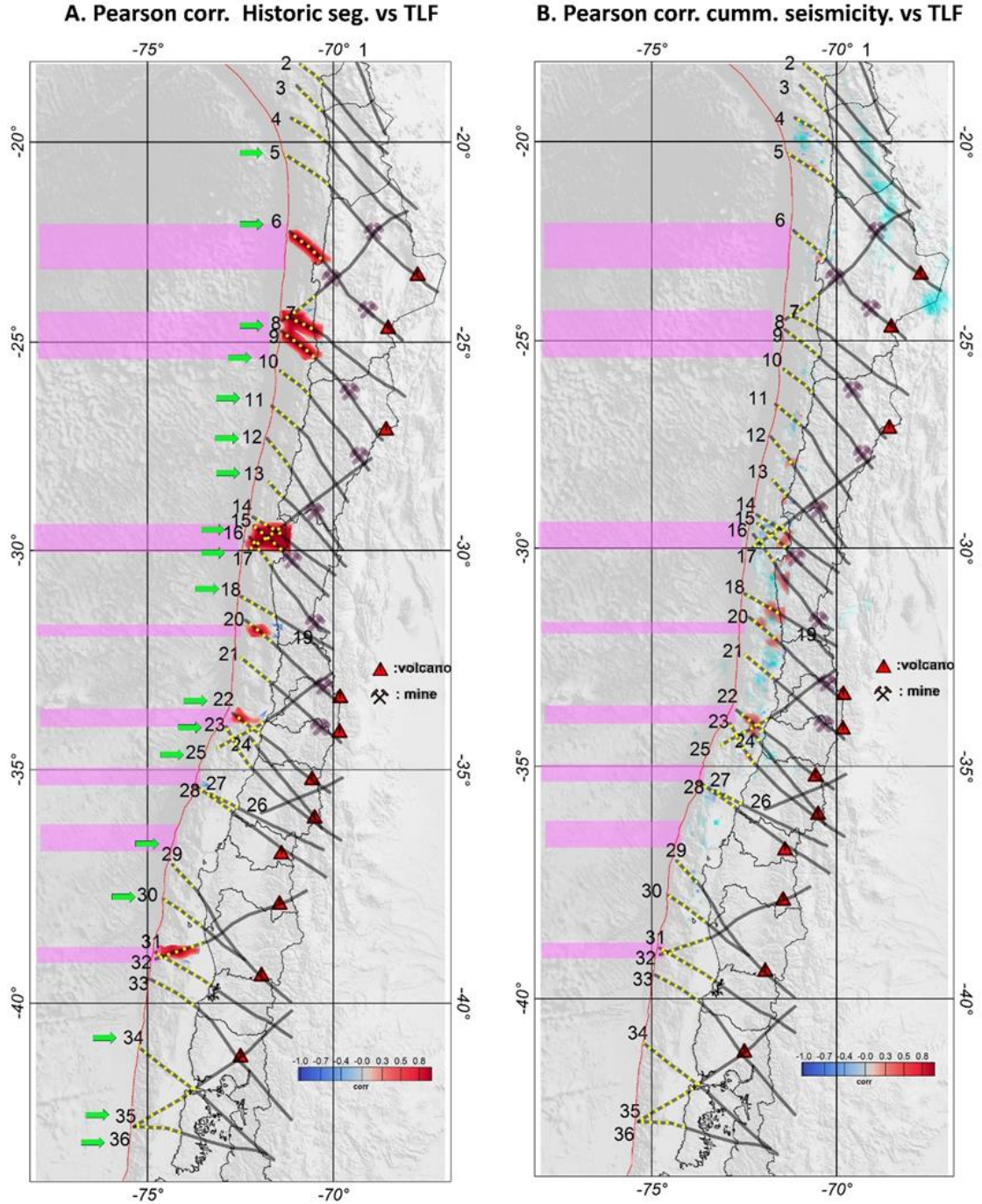
- 413 1. From the 32 relevant TLF in terms of plate coupling, 63% (20 of 32) show a high potential for a
414 barrier behaviour, 31% (10 of 32) presents some ambiguity, and only 6% (2 of 32) TLF show a poor
415 chance to become a barrier domain.
- 416 2. For the case of ambiguous potential, almost all of them present at least 2 positive correlation proxies.
- 417 3. For individual histograms, 54% histograms show a positive correlation, 28% are considered
418 ambiguous, and 18% present a negative correlation.

- 419 4. Five out of seven seismotectonic boundary segments present a strong correlation with TLF spatial
420 distribution (Figure 5). In terms of particular histogram distribution, 11 out of 13 show a positive
421 correlation and none of them show a negative correlation.
- 422 5. The cumulative interseismic seismicity (Figure 5), perhaps the weakest proxy due to the lack of
423 seismic completeness due to the very restricted time window of observation, still shows an almost
424 100% direct correlation with the TLF traces where inter-seismic activity developed (TLF 14-15-16,
425 TLF 18-20, TLF 22). In terms of the histogram distribution, shows a rather similar pattern, some
426 clear positive correlation in 6 out 18 TLF and a none conclusive solution in 12 out 18 cases.
- 427 6. The spatial distribution of the slip zones of the main megathrust events recorded in the last 50 years,
428 show a minimum positive correlation with the spatial distribution of TLF. As we can see in Figure
429 6, less than 20% of the total slip domains, potential zones of asperities, correlate positively with
430 TLF. The most conspicuous case against the rule is the slip zone of the Antofagasta 1995 that cut
431 two TLF (7: Agua Verde-Exploradora, and 8: Antofagasta-Chonchi) and partially the Tocopilla
432 2007 event (Mejillones-Llullaillaco TLF 6). Two complementary explanations are proposed in this
433 case: (1) both are small events (8Mw) compared to the other megathrust events, (2) not necessarily
434 all TLF behave as barriers all the time. For the case of Iquique 2014 event, the seaward extension of
435 Iquique TLF is not well constrained, and most likely run straight from landward segment, leaving
436 the slip zone entirely to the south of TLF 4. The remaining 80% lies outside the zone of influence
437 of TLF. In the histogram distribution, the same pattern is observed, 57% of negative Pearson
438 correlation (or positive correlation in terms of low plate coupling), 26% of ambiguous solution and
439 17% positive Pearson correlation. It is important to note that in several histograms of this proxy a
440 positive correlation is adopted when a low flat response is observed, but in the left side there is a
441 single column saturated at the maximum value for correlation -1 (most of the TLF is empty, or in
442 other words the slip zone lies outside the TLF domain).
- 443 7. In the GPS plate coupling-TLF Pearson correlation coefficient (Figure 6) 50% of the cases show a
444 negative correlation (low relative coupling), whereas 30% show some mix results, with the negative
445 correlation concentrated in the deeper parts of the coupling, and only in 20% of the cases a positive
446 correlation holds, mostly concentrated in the coupling zone of the Antofagasta 1995 and Tocopilla
447 2007 earthquakes, and probably linked with some post seismic effects. Consistently, in 18 out of 32
448 (56%) histograms responses (Figure 8), the low coupling correlation is observed, whereas in 10 out
449 of 32 (31%) the response is ambiguous, and the remaining 13% is associated with relatively high
450 GPS coupling. We acknowledge that these values are very much conditioned by the choice of the
451 threshold of 80% to separate high to low GPS coupling, but the aim is to identify less coupled
452 domains in a signal almost saturated with high values.
- 453 8. The same type of analysis was performed for the Slip Layer viscosity – TLF Pearson correlation
454 coefficient (Figure 7). In 50% of the case the correlation is opposite (low viscosity slip zones

455 corresponds with the location of TLF). In 15% of the cases, we observed mixed results, whereas in
456 35% of the cases the correspondence is positive. Similar results are obtained with histogram
457 responses (Figure 8), in 17 out of 32 (53%) the low coupling correlation is observed, whereas in 6
458 out of 32 (19%) the response is ambiguous, and the remaining 28% is associated with relative high
459 slip viscosity. One important limitation of this approach is the 1D approximation of an inherently
460 3D process. This fact is probably the main reason for its relatively low positive response compared
461 to the other proxies. Finally, figure 5c show the Pearson correlation coefficient for the distance from
462 the shelf brake to the trench. In this case, the closest shelf brake to the trench at TLF intersection is
463 a 36%, the same number of cases show an opposite behaviour and only 28% presenting mixed
464 results. In terms of the histogram distribution (Figure 8), the same tendency is observed, but with a
465 higher predominance of shorter distance shelf brake-trench (44%), whereas the opposite is observed
466 in 34% of the cases and 22% show an ambiguous response. This is the proxy that show the lowest
467 level of positiveness, probably due to the fact that other processes are also involved in the uplift of
468 the peninsula regions, for instance the density of the crust and its relative buoyancy.

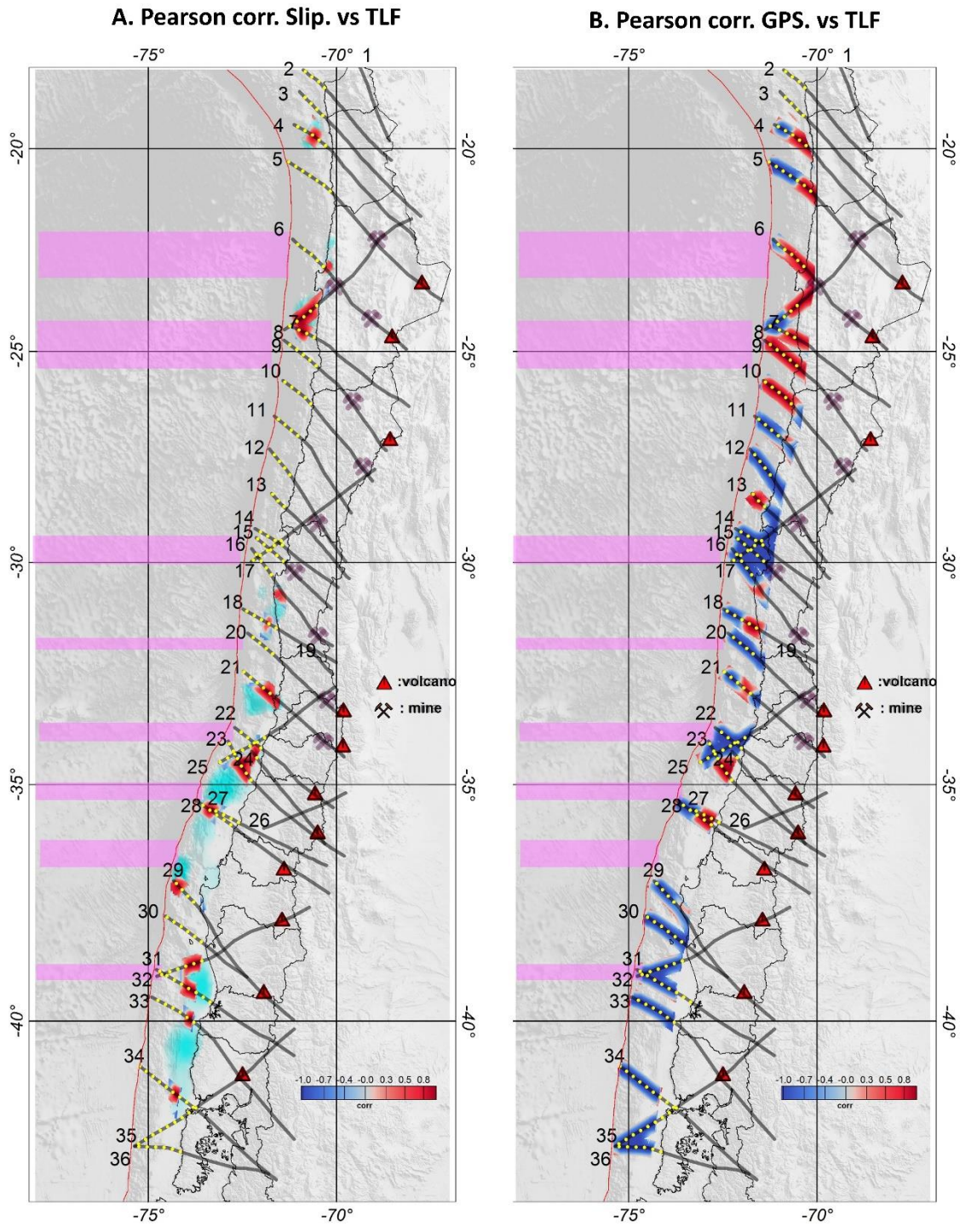
469 As we point out earlier in the text, none of the proxies by itself have the merit to account for the degree of
470 coupling along the subduction zone, and the results emanated from the Pearson correlation demonstrate that.
471 However, when we integrated the individual results 63% of the TLF can potentially behave as barrier, and only
472 in two cases (6%) chances are poor. In the remaining 31% of the cases, represented as ambiguous cases, there
473 are still some evidences of positive correlations in more than one proxy. In Figure 5a, panel A, we include a
474 reference for the TLF with high potential to become a barrier (green arrow), and we can see that in almost all
475 the cases they are consistent with the tectonic segmentation derived from the historic seismicity. One peculiar
476 distribution of potentially active barrier domains is observed between 25°-30° S, the zone with less historical
477 seismicity (Figure 2). On the other hand, not necessarily all the TLF behave as barriers, due to lack of favourable
478 orientation, depth extent, age, dip angle, fluid content among other uncertainties. Therefore, we consider that
479 the previous semiquantitative analysis including all the proxies, support the presence of a geological signal of
480 low plate coupling when a TLF is present. In the next section we propose a conceptual mechanism to explain
481 this phenomenon.

482



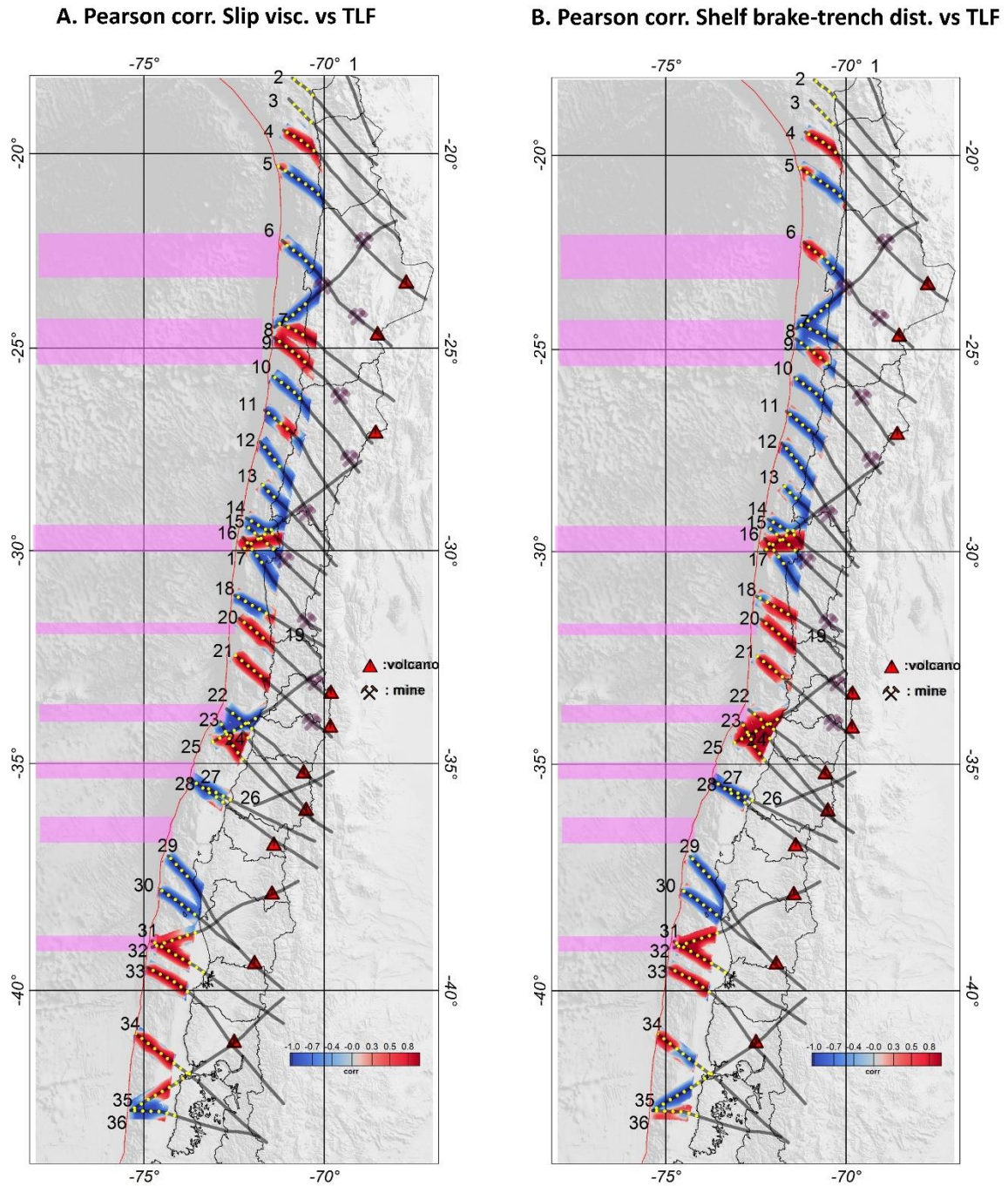
483
 484
 485
 486
 487
 488
 489

Figure 5a: Pearson correlation coefficient between TLF and (A) tectonic segmentation (from Figure 2a) and (B) cumulative seismicity (from Figure 3a). Colour code range from -1 (opposite correlation, blue colours) to 1 (direct correlation, red colours). In panel A the green arrow shows the TLF with high potential as a barrier, according with the criteria established from histograms distribution of Figure 6. Correlation is only determined in the vicinity of TLF.



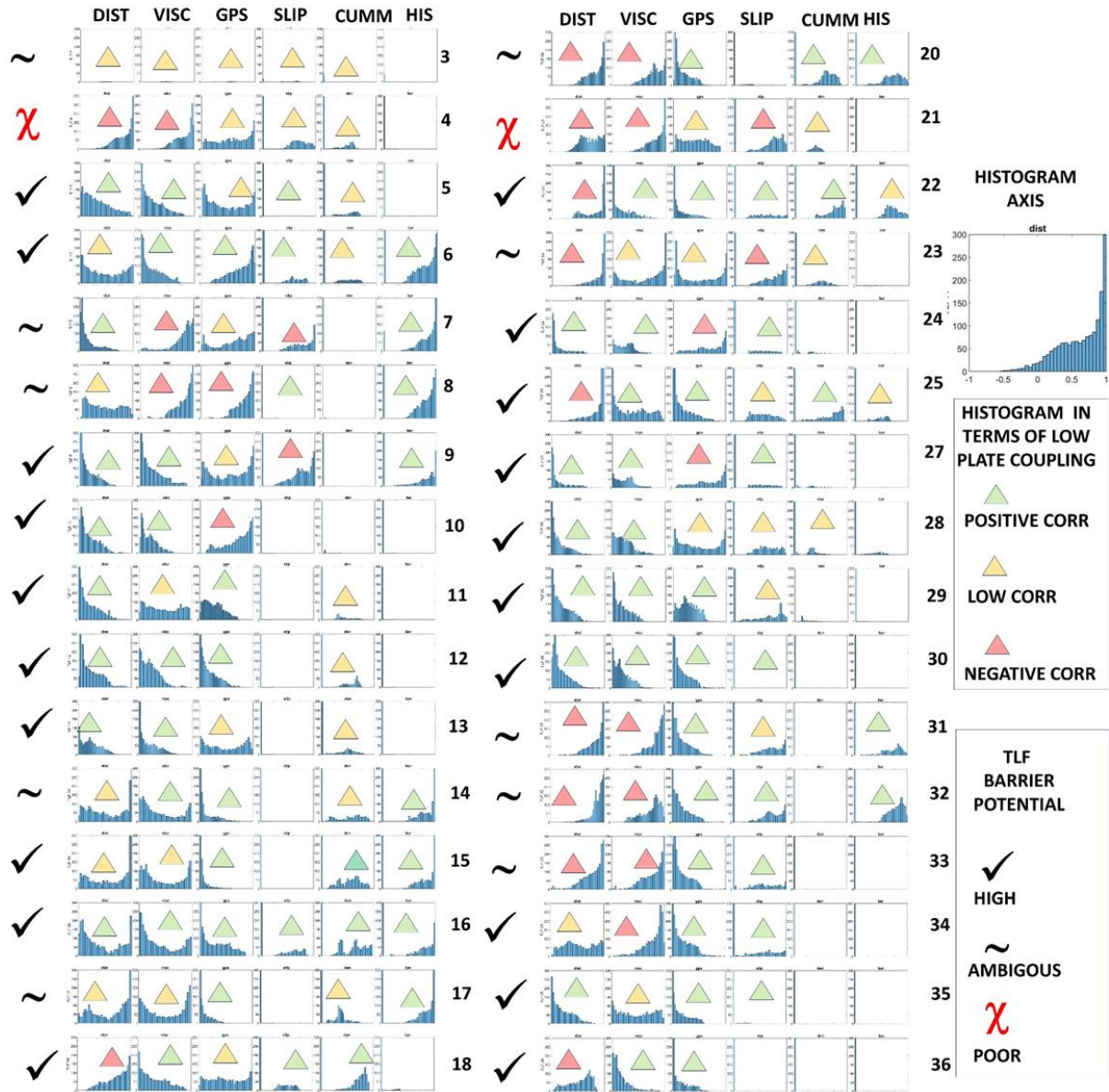
491
 492
 493
 494
 495
 496

Figure 6: Pearson correlation coefficient between TLF and (a) normalized seismic slip (from Figure 2b) and (b) GPS coupling (from Figure 4b). Colour code range from -1 (opposite correlation, blue colours) to 1 (direct correlation, red colour). Correlation is only determined in the vicinity of TLF.



498
 499
 500
 501
 502
 503
 504

Figure 7: Pearson correlation coefficient between TLF and tectonic slip viscosity (from Figure 4a) (a), and distance from the trench to the shelf brake (from Figure 3b) b). Colour code range from -1 (opposite correlation, blue colour) to 1 (direct correlation, red colour). Correlation is only determined in the vicinity of TLF.



505
506
507
508
509
510
511
512

Figure 8: Histogram diagrams for Pearson correlation in each TLF (six histograms for each TLF). Histogram interpretation and TLF qualification as a potential barrier is indicated in inlet. TLF number is indicated to the left of each panel (a good resolution of this image is provided in the supplementary material). Correlation type is indicated by triangles in each histogram, while the estimate TLF barrier potential high to poor is indicated by symbols in the left side of each histogram.

513 **3.2 A simple conceptual barrier model: misoriented TLF as a store/released of fluids during the seismic**
514 **cycle.**

515 Comparing the spatial distribution of the seaward extension of the TLF and the previously discussed first-order
516 conditioning factors of the tectonic segmentation in the Andes (chapter 2), and the cross correlation described
517 in section 4.1, we can make the following conclusions:

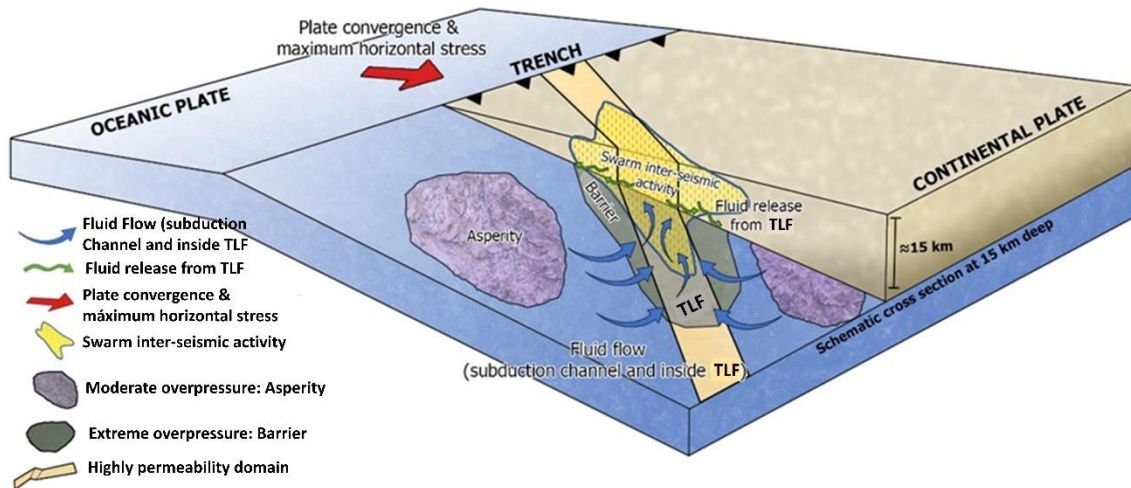
- 518 1. The coastal termination of an TLF generally occurs close to a peninsula, where the shortest trench–
519 coast distance is observed, in spatial correspondence with zones of negative RSLV (weak viscous
520 coupling), and in some cases also corresponding to zones of weak GPS coupling. However, it should
521 be noted that the degrees of coupling inferred via RSLV and GPS do not map similar observation
522 time windows, covering geological (Ma) vs seismic cycle (300–500 years) time frames, respectively.
- 523 2. During the last 60 years, slip displacements during the major megathrust earthquakes in the margin
524 of Chile tend to be bounded by the coastal termination of an TLF in their northern and southern
525 boundaries. Thus, if these slip zones represent a spatial distribution of asperities, the TLF correspond
526 to zones potentially associated with barriers, consistent with the long-term low coupling inferred
527 from RLSV, GPS plate coupling and distributions of peninsulas. the previous long-term
528 observations.
- 529 3. Cumulative seismic activity in the last 20 years tends to nucleate in the vicinity of the seaward
530 termination of the TLF, normally with the development of seismic swarms of 100–300 events of
531 medium to low magnitudes during periods of several weeks at most.
- 532 4. The geological record demonstrates that TLF are long-lived structures of high permeability in
533 comparison with the surrounding crust and most likely the underlying mantle as well, and are thus
534 potentially efficient fluid storage structures.

535 The previous observations provide the grounds to propose a simple conceptual model to understand the role
536 played by TLF in the tectonic segmentation of a convergent margin. These observations consistently show that
537 TLF in the seismogenic zone are spatially correlated with long-term and short-term evidence of weak coupling
538 behaviour. The long-term evidence involves geological processes that build up during many seismic cycles,
539 over a time frame of millions of years, including low values of slip-layer viscosities and correspondence with
540 the spatial distribution of peninsulas. The short-term evidence involves fragments of the seismic cycle over a
541 time frame of less than 500 years, characterized by weak coupling zones as inferred by inter-seismic GPS
542 observations, the flanks of slip zones of recent mega-thrust events, and the boundaries that delimit the historical
543 record of major events. Overall, these observations consistently show that TLF domains are likely candidates
544 for barrier zones.

545 From basic principles, the strength of a fault is controlled by the friction at the discontinuity plane. According
546 to Amonton’s law, the fault strength is proportional to the product of the normal stress and the static or dynamic
547 friction (e.g. Scholz, 1990). In the presence of fluids, pore pressure reduces the normal stress, thereby reducing
548 the strength of the fault (e.g. Scholz, 1990), eventually to zero if the pore pressure reaches the lithostatic pore

549 pressure. Under these supra-lithostatic fluid pressure conditions, even faults that are strongly misoriented for
550 frictional reactivation under the prevailing stress field can be reactivated, focusing the discharge of large
551 amounts of overpressured fluids and acting as a “fault-valve” (Sibson, 1990; Cox, 2016). Indeed, Cox (2016)
552 showed that, under supra-lithostatic fluid pressure conditions, the typical seismic response in the faults
553 corresponds to microseismic swarms, which, according to Sibson (2020), would concentrate at the roots of the
554 fault system. In the case of an TLF, which is a long-lived structure transecting the whole lithosphere (e.g., Lutz
555 et al., 2022), the root of the fault system at the Andean convergent margin corresponds to the subduction
556 channel. Low fault strength at subduction zones can be equated to barrier zones where convergence is mostly
557 accommodated by creep and/or micro-seismicity. The hydration of the subducting slab during its bending in the
558 outer rise region has been widely documented in different subduction margins (e.g., Holbrook et al., 1999;
559 Shillington et al., 2015; Contreras-Reyes et al., 2007; Moscoso and Grevemeyer, 2015; Ranero and
560 Sallarès, 2004; Fujie et al., 2018, among others), as has the slab’s subsequent dehydration during subduction
561 (Barriga et al., 1992; Maekawa et al., 1993; Peacock, 1993). Mantle hydrous phases (serpentinites) have also
562 been observed in forearc regions at subduction margins (e.g. Hyndman and Peacock, 2003; Xia et al., 2015;
563 Hansen et al., 2016), further demonstrating that subduction systems transport large amounts of water; however,
564 the amount of water transported is still unknown (Miller et al. 2022). On the other hand, fluid flow in porous
565 media is governed by Darcy’s law, in the opposite direction to the hydraulic head and proportional to the
566 hydraulic permeability. Numerical models (Menant et al., 2019) have been used to determine the path of
567 overpressured fluid flow along the subduction channel, and how strong/weak frictional channels condition the
568 flow (weak frictional channel zones percolate more water upwards compared to strong frictional channel zones).
569 These two domains determine the location of weak and strong coupling zones at the plate contact. Thus,
570 according to basic principles and numerical models, water concentrates in zones of high permeability.
571 The geological record on land shows that, in the Andean margin, TLF are associated with ore deposits
572 clustered at the intersection of magmatic arcs that become progressively younger eastward (Piquer et al.,
573 2016; Yáñez and Rivera, 2019; Piquer et al., 2021a; Farrar et al., 2023; Wiemer et al., 2023), covering the full
574 tectono-magmatic history during the Mesozoic and Cenozoic. Local seismic networks deployed in Northern
575 and Central Chile also show alignments of seismic activity along some TLF systems (Yáñez and Rivera,
576 2019; Piquer et al., 2019, 2021a; Sielfeld et al, 2019; Pearce et al., 2021). These long- and short-term
577 observations indicate the presence of long-lived high-permeability domains along the TLF systems in the
578 Andean margin of Northern and Central Chile. Therefore, we postulate that TLF act as fluid sinks in the
579 forearc region, following a continental-scale fault-valve behaviour, carrying the fluids released by slab
580 dehydration and transported from distal locations through the subduction channel and discharging the fluids
581 upwards and laterally through the TLF. Thus, if the proposed mechanism operates for long periods of time,
582 the fluid distribution at the plate contact should show an uneven distribution of fluid, delimitating domains of
583 weak and strong friction channels, which would act as seismic barriers and asperities, respectively. In this
584 context, the spatial distribution of TLF would be associated with barriers that delimitate the tectonic
585 segmentation. In the proposed model, tremor or swarm seismic activity represent episodic fluid release from
586 TLF that are poorly oriented with respect to the regional tectonic stress — in this case, the NW-striking fault

587 systems oriented at a high angle relative to the ENE convergence direction. This model provides a causal link
 588 between the presence of TLF in the upper plate and the distribution of barrier and asperity domains in the
 589 plate interface. A schematic cartoon of this model is presented in Figure 9.
 590 Our proposed conceptual model in which TLF's promote the development of barrier domains along the
 591 subducting margin through the enhancement of fluid pressure complement other process at subduction zones
 592 that also enhances the budget of localized fluids at the plate contact, among them the collision of aseismic
 593 ridges and fracture zones, bending of the subducting plate (e.g. Ranero et al., 2008, Ranero et al., 2005,
 594 Martinez-Loriente et al., 2019; Arai et al., 2024). In the Nazca-South America plate interaction authors had
 595 highlighted this increase in fluids at passive ridges such as the Taltal ridge 33°S (Leon-Rios et al., 2014) and
 596 the Juan Fernandez ridge 33.5°S (Garrido et al., 2002), and fracture zones such as the Challenger Fracture
 597 zone 30°S ((Poli et al., 2017; Maksymowicz, 2015). The volume of fluids in aseismic ridges is enhanced by
 598 oceanic water percolation along the thicker oceanic crust, while in fracture zones as a result of the high
 599 permeability that provides a mechanism to increase water storage prior to the subduction. These
 600 complementary mechanisms share a common origin at the subducting plate, and in the particular case of the
 601 Nazca plate they are oblique to the margin (roughly NE). Thus, the main difference with the proposed model
 602 is their along strike migration with time, while in the proposed mechanism TLF belongs to the overriding
 603 plate.



604 **Figure 9: Schematic conceptual model of fluid transport towards TLF, following different paths in the subduction**
 605 **channel, as well as upwards within the TLF. This model proposes that TLF are sink domains of slab-derived fluids**
 606 **that promote the development of barrier zones and dry out the neighbouring domains where asperities develop.**
 607 **Swarm clustering in spatial association with the TLF represents a mechanism for the quasi-creep release of energy**
 608 **within the barrier zone.**
 609

610 **3.3 Implications**
 611

612 If TLF act as low-friction domains (barriers) due to their capacity to store fluids released from the subducting
613 slab and thereby dry out neighbouring zones of the subduction channel, promoting the development of a high-
614 friction domain (asperity), we can envision a series of implications derived from the proposed model.

615 The most relevant implication is the geological control of barrier zones. This geological control exerted by high-
616 permeability domains in the continental lithosphere (TLF) implies a spatial control of barrier zones, and thus
617 the seismotectonic segmentation should be stable for several seismic cycles as long as the capacity of TLF to
618 store fluids is maintained. If this scenario is correct, the estimate of the seismic risk associated with each
619 seismotectonic segment can be assessed based on empirical fault-length laws (e.g. Anderson et al., 2016). In
620 this context, interplate seismic swarms and slow seismic events that develop in the vicinity of TLF zones would
621 be a mechanism for the steady release of seismic energy.

622 As discussed previously, several TLF have been identified in the Andean margin; however, little is known about
623 their origin, width, dip, depth extent, and capacity to behave as a water sink. Therefore, further study is needed
624 to postulate a reliable map of barrier domains in this subduction system.

625 On the other hand, seismic barriers/asperities would be conditioned by the capacity of barrier zones to
626 mobilise and store fluids, and would thus be relatively stable in space but with a variable behaviour during
627 several seismic cycles. If the age of the subducted slab conditions the water budget at the plate interface
628 (Rupke et al., 2004), the progressive age increase from south to north in this margin (from 0 to 45 Ma) would
629 be a controlling factor for the efficiency of the TLF-barrier hypothesis. Although this implication is highly
630 speculative, the historical record shows that the largest megathrust events at the margin have occurred in
631 Southern Chile, including the 9.3Mw 1960 Valdivia Earthquake, the largest event recorded worldwide.

632

633 4. Conclusions

634 Based on first order geological and geophysical observations of the Nazca-South America plate convergence
635 we propose a conceptual model to understand the tectonic segmentation in the Andean region.

636 Observations include historical seismicity and the associated seismotectonic segmentation. Major thrust events
637 occurred in the region in the last 60 years, defining domains of asperities. GPS and viscous plate coupling that
638 provide independent proxies to establish potential domains of barriers (low plate coupling) and asperities (high
639 plate coupling). Location of low plate coupling domains is further associated with the spatial distribution of
640 peninsulas (less basal erosion) and cumulative seismicity during the inter-seismic period (slow interplate
641 seismic events, creeping, associated with fluid release).

642 Key element in the model is played by trans-lithospheric faults (TLF). Landward, this TLF system concentrate
643 the occurrence of major hydrothermal ore deposits and some active volcanism, denoting their intrinsic high
644 permeability. Thus, at their seaward edge the TLF domains act as sink and release of fluids during the seismic
645 cycle. The fluid is captured from the slab through the subducting channel, and continuously release to the plate
646 contact, promoting the growth of barriers beneath them (excess of fluids), and asperities laterally (reduction in
647 fluid content).

648 If the interaction of first order continental structures and the fluid content of the subducting slab plays a
649 central role in the seismotectonic segmentation of convergence zones, a carefully understanding of the

650 overriding plate geology and associated structures could be instrumental to better understand the associated
651 seismic risk.

652

653 **Competing interests:** The contact author has declared that none of the authors has any competing interests.

654 **Acknowledge:** This research was partially supported by Fondef project D10I1027. J.P. acknowledges support
655 from ANID-FONDECYT grant 11181048 and Amira Global P1249 project. We also would like to thanks Prof.
656 Booth-Rea and one anonymous reviewer for their valuable observations. We think the paper has been greatly
657 improved with the observations made by both reviewers.

658 **Data Availability Statement:** The data used in this paper is derived from published papers, indicated in the
659 text, and topographic/bathymetric data extracted from public source, ETOPO 2022. DOI: 10.25921/fd45-gt74.

References

- Aki, K.: Asperities, barriers, characteristic earthquakes and strong motion prediction. *Journal of Geophysical Research* 89: doi: 10.1029/JB089iB07p05867, 1984.
- Angermann, D., Klotz J., Reigber C., Space-geodetic estimation of the Nazca–South America Euler vector. *Earth and Planetary Science Letters*, 171(3), 329–334. [https://doi.org/10.1016/S0012-821X\(99\)00173-9](https://doi.org/10.1016/S0012-821X(99)00173-9), 1999.
- 665 Arai, R., Shiraishi, K., Nakamura, Y. et al, Thick slab crust with rough basement weakens interplate coupling in the western Nankai Trough. *Earth Planets Space* 76, 73, <https://doi.org/10.1186/s40623-024-02025-4>, 2024.
- Arriagada, C., Roperch P., Mpodozis C., Dupont-Nivet G., Cobbold P.R., Chauvin A., Cortés J., Paleogene clockwise tectonic rotations in the forearc of central Andes, Antofagasta region, northern Chile. *Journal of Geophysical Research: Solid Earth*, 670 108(B1), 2003.
- Aron, F., Allmendinger R., Cembrano J., González G., and Yáñez G., Permanent Forearc Extension and Seismic Segmentation: Insights from the 2010 Maule Earthquake, Chile, *J. Geophys. Res.*,doi:10.1029/2012JB009339, 2013.
- Avouac, J.P., Dynamic Processes in Extensional and Compressional Set–ings - Mountain Building: From Earthquakes to Geological Deformation, *Treatise on Geophysics*, 6 , 377 – 439, 2007.
- 675 Barrientos S.E. , Ward S.N., The 1960 Chile earthquake: inversion for slip distribution from surface deformation, *Geophysical Journal International*, Volume 103, Issue 3, Pages 589–598, <https://doi.org/10.1111/j.1365-246X.1990.tb05673.x>, 1990.
- Barriga, F. J. A. S., Fyfe, W.S. , Landefeld, L.A., Ribeiro, A., Mantle eduction: Tectonic fluidisation at depth. *Earth Science Reviews* 32, 123-9, 1992.
- Bilek, S. L., S.Y. Schwartz, H.R. DeShon, (2003). Control of seafloor roughness on earthquake rupture behavior. *Geology* 31, 680 455–458
- W. F. Brace, Byerlee, J.D. ,Stick-Slip as a Mechanism for Earthquakes.*Science*153,990 - 992,DOI:10.1126/science.153.3739.990, 1966.
- Burridge, R., Knopoff, L., Model and theoretical seismicity. *Bulletin of the Seismological Society of America*; 57 (3): 341–371. doi: <https://doi.org/10.1785/BSSA0570030341>, 1967.
- 685 Bürgmann, R., Kogan, M. G., Steblov, G. M., Hilley, G., Levin, V. E., & Apel, E., Interseismic coupling and asperity distribution along the Kamchatka subduction zone. *Journal of Geophysical Research*, **110**, B07405. <https://doi.org/10.1029/2005JB003648>, 2005.
- Cahill, T., Isacks, B.L., Seismicity and shape of the subducted Nazca Plate, *Journal of Geophysical Research*, vol 97, B12, 17503-17529, 1992.

- 690 Calle-Gardella, D., Comte, D., Farías, M. et al., Three-dimensional local earthquake tomography of pre-Cenozoic structures in the coastal margin of central Chile: Pichilemu fault system. *J Seismol* 25, 521–533 <https://doi.org/10.1007/s10950-021-09989-w>, 2021.
- Carretier, S., Regard, V., Vassallo, R., Aguilar, G., Martinod, J., Riquelme, R., ... & Lagane, C, Slope and climate variability control of erosion in the Andes of central Chile. *Geology*, 41(2), 195-198, 2013.
- 695 Cembrano, J., Lara, L., The link between volcanism and tectonics in the southern volcanic zone of the Chilean Andes: A review, *Tectonophysics* 471, 96–113, 2009.
- Chernicoff, C.J., Richards, J.P., Zappettini, E.O., Crustal lineament control on magmatism and mineralization in northwestern Argentina: geological, geophysical, and remote sensing evidence. *Ore Geology Reviews* 21, 127-155, 2002.
- Chlieh, M. , De Chabalier, J. B., Ruegg, J. C., Armijo, R. Dmowska,, R. , Campos, J., Feigl, K.L.,. Crustal deformation and
700 fault slip during the seismic cycle in the North Chile subduction zone, from GPS and InSAR observations, *Geophysical Journal International* Volume 158, Issue 2 p. 695-711, 2004.
- Chlieh, M., Avouac, J. P., Sieh, K., Natawidjaja, D. H., & Galetzka, J., Heterogeneous coupling of the Sumatran megathrust constrained by geodetic and paleogeodetic measurements. *Journal of Geophysical Research*, **113**, B05305. <https://doi.org/10.1029/2007JB004981>, 2008.
- 705 Comte, D., Eisenberg, A., Lorca, E., Pardo, M., Ponce, L., Saragoni, R., Singh, S.K., Suárez, G., The 1985 Central Chile Earthquake: A Repeat of Previous Great Earthquakes in the Region?, *Science*, 07-25 233(4762): 449-453, 1986.
- Contreras-Reyes, E., Grevemeyer, I., Flueh, E.R., Scherwath, M., and Heesemann, M., Alteration of the subducting oceanic lithosphere at the southern central Chile trench–outer rise, *Geochem. Geophys. Geosyst.*, 8, Q07003, doi:10.1029/2007GC001632, 2007.
- 710 Cox, S.F., Injection-driven swarm seismicity and permeability enhancement: implications for the dynamics of hydrothermal ore systems in high fluid-flux, overpressured faulting regimes. *Economic Geology* 111, pp. 559–587, 2016.
- Creixell, C., Parada, M. A., Morata, D., Vásquez, P., Pérez de Arce, C., Arriagada, C., Middle-Late Jurassic to Early Cretaceous transtension and transpression during arc building in Central Chile: evidence from mafic dike swarms, *Andean Geol.* 38, 37-63, 2011.
- 715 Delouis, B., Monfret, T., Dorbath, L., Pardo, M., Rivera, L., Comte, D., Haessler, H., Caminade, J.P., Ponce, L., Kausel, E., Cisternas, A., The Mw = 8.0 Antofagasta (northern Chile) earthquake of 30 July 1995: A precursor to the end of the large 1877 gap. *Bulletin of the Seismological Society of America*, 87 (2): 427–445. doi: <https://doi.org/10.1785/BSSA0870020427>, 1997.
- Delouis, B., Nocquet, J.M., Vallée, M., Slip distribution of the February 27, 2010 Mw = 8.8 Maule Earthquake, central Chile, from static and high-rate GPS, InSAR, and broadband teleseismic data, *Geophys. Res. Lett.*, 37, L17305,
720 doi:10.1029/2010GL043899, 2010.
- Demets, C., Gordon, R., Argus, D., Stein, S., Current Plate Motions. *Geophysical Journal International*. 101– 425 - 478. 10.1111/j.1365-246X.1990.tb06579.x, 1990.

- 725 Espinoza, M., Montecino, D., Oliveros, V., Astudillo, N., Vásquez, P., Reyes, R., Celis, C., González, R., Contreras, J., Creixell, C., Martínez, A., The synrift phase of the early Domeyko Basin (Triassic, northern Chile): Sedimentary, volcanic, and tectonic interplay in the evolution of an ancient subduction-related rift basin. *Basin Research* 31, 4-32, 2019.
- Fariás M., D. Comte, D., Roecker, S., Carrizo, D., Pardo, M., Crustal extensional faulting triggered by the 2010 Chilean Earthquake: The Pichilemu Seismic Sequence: *Tectonics*, v. 30, TC6010, doi:10.1029/2011TC002888, 2011.
- 730 Farrar, A.D., Cooke, D.R., Hronsky, J.M.A., Wood, D.G., Benavides, S., Cracknell, M.J., Banyard, J.F., Gigola, S., Ireland, T., Jones, S.M., Piquer, J, A Model for the lithospheric architecture of the Central Andes and the localization of giant porphyry copper deposit clusters. *Economic Geology* 118 (6), 1235–1259, doi: 10.5382/econgeo.5010, 2023.
- Fedotov, S. A., On seismic cycle, possibility of quantitative seismic regionalization and long-term seismic prediction. In *Seismic Zoning of the USSR* (ed. S. Medvedev) (Nauka, Moscow) pp. 121-150, 1968.
- Fischer, T., Control estructural sobre la circulación de magmas y fluidos hidrotermales Miocenos y Cuaternarios en el sector de La Invernada, Región del Maule, Chile. Valdivia: Universidad Austral de Chile, 314, 2021.
- 735 Forsyth, D., Yang, W., Y., Mangriotis, M.D., Shen, Y., Coupled seismic slip on adjacent oceanic transform faults. *Geophysical Research Letters*, 30(12), 2003.
- Fujie, G., Kodaira, S., Kaiho, Y., et al., Controlling factor of incoming plate hydration at the north-western Pacific margin. *Nat Commun* 9, 3844, 2018.
- Gana, P., Wall, R., Gutiérrez, A., Mapa Geológico del Área de Valparaíso – Cuarcaví. Regiones de Valparaíso y
740 Metropolitana, Mapas Geológicos N°1, Escala 1:100.000. Servicio Nacional de Geología y Minería, Chile, 1996.
- Garrido, I., Cembrano, J., Siña, A., Stedman, P., Yáñez, G., High magma oxidation state and contractional deformation: key factors in the generation of Andean porphyry copper deposits, Central Chile (31-34°S). *Revista Geológica de Chile*, Vol. 29, No. 1, p. 3-14, 2002.
- 745 Geersen, J., Ranero, C., Barchhausen, U., Subducting seamounts control intraplate coupling and seismic rupture in the 2014 Iquique earthquake area. *Nat Commun* 6, 8267. <https://doi.org/10.1038/ncomms9267>, 2015.
- Giambiagi, L., Álvarez, P., Creixell, C., Mardonez, D., Murillo, I., Velásquez, R., Lossada, A., Suriano, J., Mescua, J., Barrionuevo, M., Cenozoic Shift From Compression to Strike-Slip Stress Regime in the High Andes at 30°S, During the Shallowing of the Slab: Implications for the El Indio/Tambo Mineral District. *Tectonics*, Vol. 36, Issue 11. <https://doi.org/10.1002/2017TC004608>, 2017.
- 750 Glodny, J., Echtler, H., Collao, S., Ardiles, M., Burón, P., Figueroa, O., Differential Late Paleozoic active margin evolution in South-Central Chile (37°S-40°S) -The Lanalhue Fault Zone. *Journal of South American Earth Sciences*, 26, 4, 397-411 DOI: 10.1016/j.jsames.2008.06.001, 2008.
- Gutscher, M.A., Malavielle, J., Lallemand, S., Collot, J.Y., Tectonic segmentation of the north Andean margin: impact of the Carnegie Ridge collision, *Earth and Planetary Science Letters*, 168, 255-270, 1999.

- 755 González-Vidal D., Moreno, M., Sippl, C., Baez, J. C., Ortega-Culaciati, F., Lange, D., et al, Relation between oceanic plate structure, patterns of interplate locking and microseismicity in the 1922 Atacama seismic gap. *Geophysical Research Letters*, 50, e2023GL103565. <https://doi.org/10.1029/2023GL103565>, 2013.
- Haberland, C., Rietbrock, A., Lange, D., Bataille, K., Hofmann, S., Interaction between forearc and oceanic plate at the south-central Chilean margin as seen in local seismic data. *Geophysical Research Letters* 33: 1-5, 2006.
- 760 Hansen, S., Schmandt, B., Levander, A., et al., Seismic evidence for a cold serpentinized mantle wedge beneath Mount St Helens. *Nat Commun* 7, 13242. <https://doi.org/10.1038/ncomms13242>, 2016.
- Hayes G., Slab2 – A Comprehensive Subduction Zone Geometry Model: U.S. Geological Survey data release, <https://doi.org/10.5066/F7PV6JNV>, 2018.
- Hayes G., Herman, M., Barnhart, W., et al., Continuing megathrust earthquake potential in Chile after the 2014 Iquique earthquake. *Nature* 512, 295–298. <https://doi.org/10.1038/nature13677>, 2014.
- 765 Heidarzadeh, M., Murotani, S., Satake, K., Ishibe, T., Gusman, A.R., Source model of the 16 September 2015 Illapel, Chile Mw 8.4 earthquake based on teleseismic and tsunami data. *Geophys. Res. Lett.* 43, 643–650, 2016.
- Hyndman, R.D., Peacock, S.M., Serpentinization of the forearc mantle, *Earth and Planetary Science Letters* 212, 417-432, 2002.
- 770 Kay, S.M., Mpodozis, C., Magmatism as a probe to the Neogene shallowing of the Nazca plate beneath the modern Chilean flat slab. *Journal of South American Earth Sciences* 15, 39-57, 2002.
- Kimura, G., Yamaguchi, A., Masataka, M., Upper-plate tectonic hysteresis and segmentation of the rupture area during seismogenesis in subduction zones—A case study of the Nankai "rough", *Geology and Tectonics of Subduction Zones: A Tribute to Gaku Kimura*, Timothy Byrne, Michael B. Underwood, III, Donald Fisher, Lisa McNeill, Demian Saffer, Kohtaro Ujije, Asuka Yamaguchi, [https://doi.org/10.1130/2018.2534\(05\)](https://doi.org/10.1130/2018.2534(05)), 2018.
- 775 Ujije, Asuka Yamaguchi, [https://doi.org/10.1130/2018.2534\(05\)](https://doi.org/10.1130/2018.2534(05)), 2018.
- Kley, J., Monaldi, C.R., Salfity, J.A, Along-strike segmentation of the Andean foreland: causes and consequences, *Tectonophysics*, Volume 301, Issues 1–2, Pages 75-94, ISSN 0040-1951, [https://doi.org/10.1016/S0040-1951\(98\)90223-2](https://doi.org/10.1016/S0040-1951(98)90223-2), 1999.
- Kohler P. A., *Geología del Complejo Volcánico Laguna del Maule y su control sobre la deformación cortical*, Undergraduate thesis. Concepción: Universidad de Concepción, 225, 2016.
- 780 Koper, K. D., Hutko, A.R., Lay, T., and Sufri, O., Imaging short-period seismic radiation from the 27 February 2010 Chile (Mw 8.8) earthquake by back-projection of P, PP, and PKIKP waves, *J. Geophys. Res.* 117, B02308, 2012.
- Lamb, S., Davis, P., Cenozoic climate change as a possible cause for the rise of the Andes. *Nature*. 425. 792-7. [10.1038/nature02049](https://doi.org/10.1038/nature02049), 2003.
- 785 Lanza, F., Tibaldi, A., Bonali, F.L., Corazzato, C., Space–time variations of stresses in the Miocene–Quaternary along the Calama–Olacapato–El Toro Fault Zone, Central Andes. *Tectonophysics* 593, 33-56, 2013.

- Lara, L., Lavenu, A., Cembrano, J., Rodríguez, C., Structural controls of volcanism in transversal chains: resheared faults and neotectonics in the Cordón Caulle–Puyehue area (40.5°S), Southern Andes. *Journal of Volcanology and Geothermal Research* 158, 70–86, <https://doi.org/10.1016/j.jvolgeores.2006.04.017>, 2006.
- 790 Lay, T., Kanamori, H., Ruff, L., The asperity model and the nature of large subduction zone earthquake occurrence, *Earthquake Prediction Research*, 1, 3-71, 1982.
- Lay, T., Bilek, S.L., Anomalous earthquake ruptures at shallow depths on subduction zone megathrusts, in: *The Seismogenic Zone of Subduction Thrust Faults*, Edited by T. H. Dixon and J. C. Moore, Columbia University Press, New York, pp. 476-511, 2007.
- 795 Lay, T., C. Ammon, J., Kanamori, H., Koper, K.D., Sufri, O., Hutko A.R., Teleseismic inversion for rupture process of the 27 February 2010 Chile (Mw 8.8) earthquake, *Geophys. Res. Lett.*, 37, L13301, doi:10.1029/2010GL043379, 2010.
- Lay, T., Yue, H.E.E, Brodsky, E. E. , An C., The 1 April 2014 Iquique, Chile Mw 8.1 earthquake rupture sequence, *Geophys. Res. Lett.*, 41, doi:10.1002/2014GL060238, 2014.
- Lay, T., The surge of great earthquakes from 2004 to 2014, *Earth and Planetary Sci. Lett.*, Invited Frontiers Paper, 409, 133-800 146, 2015.
- Lee, S.J., Yeh, T.Y. , Lin, T.C., Lin, Y.Y. , Song, T.R., Huang, B. STwo-stage composite megathrust rupture of the 2015 Mw8.4 Illapel, Chile, earthquake identified by spectral-element inversion of teleseismic waves, *Geophys. Res. Lett.*, 43, 4979– 4985, doi:10.1002/2016GL068843, 2016.
- Leon-Rios, S., Reyes-Wagner, V., Calle-Gardella, D., Rietbrock, A., Roecker, S., Maksymowicz, A., & Comte, D.,
805 Structural characterization of the Taltal segment in northern Chile between 22°S and 26°S using local earthquake tomography. *Geochemistry, Geophysics, Geosystems*, 25, e2023GC011197. <https://doi.org/10.1029/2023GC011197>, 2024.
- Li, L., T. Lay, Cheung, K. F., Ye L., Odellingdeling of teleseismic and tsunami wave observations to constrain the 16 September 2015 Illapel, Chile, MW 8.3 earthquake rupture process, *Geophysical Research Letters*, 43, 4303-4312, doi:10.1002/2016GL068674, 2016.
- 810 Lin, Y. N. N., Sladen, A., Ortega-Culaciati, F., Simons, M., Avouac, J.P., Fielding, E.J., Socquet,, A., Coseismic and postseismic slip associated with the 2010 Maule Earthquake, Chile: Characterizing the Arauco Peninsula barrier effect. *Journal of Geophysical Research: Solid Earth*, 118(6), 3142-3159, 2013.
- Lorito, S., Romano, F., Atzori S., et al., Limited overlap between the seismic gap and coseismic slip of the great 2010 Chile earthquake. *Nature Geosci* 4, 173–177 <https://doi.org/10.1038/ngeo1073>, 2011.
- 815 Loveless, J. P., Meade, B. J., Stress modulation on the San Andreas fault by interseismic fault system interactions. *Geology*, 39, 1035–1038. <https://doi.org/10.1130/G32215.1>, 2011.
- Lutz, B.M., Axen, G.J., van Wijk, J.W., Phillips, F.M., Whole-lithosphere shear during oblique rifting. *Geology* 50, 412–416, <https://doi.org/10.1130/G49603.1>, 2022.
- Maekawa H., Shzui, M., Ishii, T., Freyer P., Pearce J.A., Blueshist metamorphism in active subduction zone, *Nature*, v. 364,
820 p. 520-523, 1993.

- Maksymowicz A., The geometry of the Chilean continental wedge: Tectonic segmentation of subduction processes off Chile, *Tectonophysics* Volume 659, 30 September 2015, Pages 183-196, <https://doi.org/10.1016/j.tecto.2015.08.007>, 2015.
- Martínez-Loriente, S., Sallarès, V., R. Ranero, C., B. Ruh, J., Barckhausen, U., Grevemeyer, I., Bangs, N., Influence of incoming plate relief on overriding plate deformation and earthquake nucleation: Cocos Ridge subduction (Costa Rica). *Tectonics*, 38, 4360–4377. <https://doi.org/10.1029/2019TC005586>, 2019.
- Marrett, R.A., Allmendinger, R.W., Alonso, R.N., Drake, R.E., Late Cenozoic tectonic evolution of the Puna Plateau and adjacent foreland, northwestern Argentine Andes. *Journal of South American Earth Sciences*, Vol. 7, N°2, pp179-207, 1994.
- McCaffrey, R., Stein, S., Freymueller, J., Crustal block rotations and plate coupling. *Geodynamics Series*, **30**, 101–122, 2002.
- McCuaig, T.C., Hronsky, J.M.A., The mineral system concept: the key to exploration targeting. Society of Economic Geologists, Special Publication 18, 153-176, 2014.
- Melgar, D., Fan, W., Riquelme, S. Gengm, J., Liang, C., Fuentes, M., Vargas, G., Allen, R. M., Shearer, P. M., Fielding, E. J., Slip segmentation and slow rupture to the trench during the 2015, Mw8.3 Illapel, Chile earthquake, *Geophys. Res. Lett.*, 43, 961–966, doi:10.1002/2015GL067369, 2016.
- Melnick, D., Echtler, H.P., Morphotectonic and Geological digital Map Compilations of the South-Central Chile (36°-42°S), In: The Andes active subduction orogeny, Onken et al. editors, *Frontiers in Earth Sciences*, ,565-568, Elsevier, 569p, 2006.
- Melnick, D., Bookhagen, B., Strecker, M., Echtler, H., Segmentation of megathrust rupture zones from fore-arc deformation patterns over hundreds to millions of years, Arauco Peninsula, Chile. *Journal of Geophysical Research*. 114. 10.1029/2008JB005788., 2009.
- Menant, A., Angiboust, S. Gerya, T. et al., Transient stripping of subducting slabs controls periodic forearc uplift. *Nat Commun* 11, 1823. <https://doi.org/10.1038/s41467-020-15580-7>, 2020..
- Mendoza, C., Hartzel, S., Monfret, T., Wide-band analysis of the 3 March 1985 central Chile earthquake: Overall source process and rupture history, *Bull. Seismol. Soc. Am.*, 84, 269– 283, 1994.
- Métois, M., Socquet, A., Vigny, C., Interseismic coupling, segmentation and mechanical behavior of the Central Chile subduction zone. *Journal of Geophysical Research*. 117. 10.1029/2011JB008736, 2012.
- Métois, M., Vigny, C., Socquet, A., Interseismic Coupling, megathrust earthquakes and seismic swarms along the Chilean Subduction Zone (38°–18°S). *Pure and Applied Geophysics*, **173**, 1431–1449. <https://doi.org/10.1007/s00024-016-1280-5>, 2016.
- Miller, N. C., Lizarralde, D., Collins, J.A., Holbrook, W.S., Van Avendonk, H.J. Limited mantle hydration by bending faults at the Middle America Trench. *Journal of Geophysical Research: Solid Earth*, 126, e2020JB020982. <https://doi.org/10.1029/2020JB020982>, 2021.
- Moggi, K. Seismic activity and earthquake prediction, *Proc. Earthquake Pred. Res. Syrup.*, 1976, 203-214, Tokyo, 1977.
- Moggi, K., *Earthquake Prediction* (Academic Press, Tokyo), 1985.
- Moreno, M., Rosenau, M., Oncken, O., 2010 Maule earthquake slip correlates with pre-seismic locking of Andean subduction zone. *Nature*, **467**, 198–202. <https://doi.org/10.1038/nature09349>, 2010.

- 855 Moreno, M., Melnick, D., Rosenau, M., Baez, J., Klotz J., Oncken, O., et al., Toward understanding tectonic control on the Mw 8.8 2010 Maule Chile earthquake. *Earth and Planetary Science Letters*, 321, 152-165, 2012.
- Moreno, M., Haberland, C., Oncken, O. et al. Locking of the Chile subduction zone controlled by fluid pressure before the 2010 earthquake. *Nature Geosci* 7, 292–296, 2014.
- Molina, D., Tassara, A., Abarca, R., Melnick, R.D., Madella. A., Frictional segmentation of the Chilean megathrust from a
860 multivariate analysis of geophysical, geological, and geodetic data. *Journal of Geophysical Research: Solid Earth*, 126, e2020JB020647, <https://doi.org/10.1029/2020JB020647>, 2021.
- Moscoso, E., Grevemeyer, I, Bending-related faulting of the incoming oceanic plate and its effect on lithospheric hydration and seismicity: A passive and active seismological study offshore Maule, Chile. *Journal of Geodynamics*. 90. 58-70. 10.1016/j.jog.2015.06.007, 2015.
- 865 Mpodozis, C., Ramos, V., The andes of Chile and Argentina. Circum Pacific Council Publications, 1990.
- Müller, R. D., Zahirovic, S. , Williams, S.E., Cannon, J., Seton, M, Bower, D.J., Tetley, M.G., Heine, C., Le Breton, E., Liu, S., , Russell, S.H.J., Yang, T., Leonard, J., Gurnis M., A global plate model including lithospheric deformation along major rifts and orogens since the Triassic. *Tectonics*, vol. 38, 2019.
- Nealy, J. L., Herman, M. W. , Moore, G. L. , Hayes, G. P. , Benz, H. M. , Bergman, E. A., Barrientos, S.E., 2017 Valparaíso
870 earthquake sequence and the megathrust patchwork of central Chile, *Geophysical Research Letters* 44, doi: 10.1002/2017GL074767, 2017.
- Niemeyer, H., Berrios, H., de la Cruz, R., Temperatures of formation in Triassic cataclasites of Cordillera Domeyko, Antofagasta, Chile. *Rev. Geol. Chile* 31, 3-18, 2004.
- NOAA National Centers for Environmental Information, ETOPO 2022 15 Arc-Second Global Relief Model. NOAA National
875 Centers for Environmental Information. [Dataset]. DOI: 10.25921/fd45-gt74, 2022.
- Okada, Y., Surface Deformation due to Shear and Tensile Faults in a Half-Space. *Bulletin of the Seismological Society of America*, 75, 1135-1154, 1985.
- Palacios, C., Ramírez, L.A., Townley, B., Solari, M., Guerra, N., The role of the Antofagasta–Calama Lineament in ore deposit deformation in the Andes of northern Chile. *Mineralium Deposita* 42, 301-308, 2007.
- 880 Pasten-Araya, F., Salazar, P., Ruiz, S., Rivera, E., Potin, B., Maksymowicz,A., et al., Fluids along the plate interface influencing the frictional regime of the Chilean subduction zone, northern Chile. *Geophysical Research Letters*, 45. <https://doi.org/10.1029/2018GL079283>, 2018.
- Peacock S.M., Large-scale hydration of the lithosphere above subducting slabs, *Chemical Geology*, Volume 108, Issues 1–4, Pages 49-59, ISSN 0009-2541, [https://doi.org/10.1016/0009-2541\(93\)90317 C](https://doi.org/10.1016/0009-2541(93)90317 C), 1993.
- 885 Pearce, R.K., Sánchez de la Muela, A. , Moorkamp, M., Hammond, J.O.S ., Mitchell T.M., Cembrano, J. Araya-Vargas, J., Meredith, P.G., , Iturrieta, P. Pérez-Estay, N., Marshall, N.R., Smith, J., Yañez, G., Griffith, A., Marquardt, C., , Stanton-Yonge, A., Núñez, R., Reactivation of fault systems by compartmentalized hydrothermal fluids in the Southern Andes revealed by magnetotelluric and seismic data. *Tectonics* 39, e2019TC005997, 2020..

- Peña, M., Origen de las Rotaciones Tectónicas en el Márgen Occidental de América del Sur: Influencia de Heterogeneidades en las Placas de Nazca y Sudamericana. Tesis para Optar al Grado de Doctor en Ciencias, Mención Geología. Inédito, 214 p. Universidad de Chile, Facultad de Ciencias Físicas Y Matemáticas, Departamento de Geología. Chile, 2022.
- Perrin, C., Waldhauser, F., Scholz, C. H., The shear deformation zone and the smoothing of faults with displacement. *Journal of Geophysical Research: Solid Earth*, 126, e2020JB020447. <https://doi.org/10.1029/2020JB020447>, 2021.
- Philibosian, B., Meltzner, A.J., Segmentation and supercycles: A catalog of earthquake rupture patterns from the Sumatran Sunda Megathrust and other well-studied faults worldwide. *Quaternary Science Reviews* 241, <https://doi.org/10.1016/j.quascirev.2020.106390>, 2020.
- Poli P., Maksymowicz, A., Ruiz, S., The Mw 8.3 Illapel earthquake (Chile): Preseismic and postseismic activity associated with hydrated slab structures. *Geology*, 45 (3): 247–250. doi: <https://doi.org/10.1130/G38522.1>, 2017.
- Piquer, J., Skármeta, J., Cooke, D.R., Structural evolution of the Río Blanco-Los Bronces district, Andes of central Chile: controls on stratigraphy, magmatism and mineralization. *Economic Geology* 110, 1995-2023, 2015.
- Piquer, J., R.F. Berry, R.J. Scott, D.R. Cooke, Arc-oblique fault systems: their role in the Cenozoic structural evolution and metallogensis of the Andes of central Chile. *Journal of Structural Geology* 89, 101–117, <https://doi.org/10.1016/j.jsg.2016.05.008>, 2016.
- Piquer, J.; Yáñez G., Rivera O., Cooke D., Long-lived damage zones associated with fault intersections in the Andes of Central Chile. *Andean Geology* 46 (2): [doi:<http://dx.doi.org/10.5027/andgeoV46n2-3106>], 2019.
- Piquer J., Rivera, O., Yáñez, G., Oyarzun, N., The Piuquencillo Fault System: a long-lived, Andean-transverse fault system and its relationship with magmatic and hydrothermal activity, *Solid Earth*, (<https://doi.org/10.5194/se-2020-142>), 2021a.
- Piquer, J., Sanchez-Alfaro, P., Pérez-Flores, P., A new model for the optimal structural context for giant porphyry copper deposit formation. *Geology* 49, 597-601, <https://doi.org/10.1130/G48287.1>, 2021b.
- Poli P., Maksymowicz, A., Ruiz, S., The Mw 8.3 Illapel earthquake (Chile): Preseismic and postseismic activity associated with hydrated slab structures. *Geology*. 45. [10.1130/G38522.1](https://doi.org/10.1130/G38522.1), 2017.
- Pritchard, M.E., Simons, M., Rosen, P.A., Hensley, S., Webb, F.H., Co-seismic slip from the 1995 July 30 Mw= 8.1 Antofagasta, Chile, earthquake as constrained by InSAR and GPS observations. *Geophysical Journal International*, 150: 362-376. <https://doi.org/10.1046/j.1365-246X.2002.01661.x>, 2002.
- Radic, J.P., Las cuencas cenozoicas y su control en el volcanismo de los Complejos Nevados de Chillán y Copahue-Callaqui (Andes del Sur, 36-39° S). *Andean Geology* 37 (1): 220-246. Doi: [10.5027/andgeoV37n1-a09](https://doi.org/10.5027/andgeoV37n1-a09), 2010.
- Ramos, V., The Basement of Central Andes: The Arequipa and Related Terranes. *Annu. Rev. Earth Planet. Sci.*, 36, pp. 289-324, 2008.
- Ramos, V., Kay, S., Overview of the tectonic evolution of southern central Andes of Mendoza and Neuquén (35°-39° S latitude). *Geological Society of America, Special Paper* 407, 2006.
- Ranero, C., Sallares V., Geophysical evidence for hydration of the crust and mantle of the Nazca plate during bending at the north Chile Trench. *Geology*. 32. [10.1130/G20379.1](https://doi.org/10.1130/G20379.1), 2004.

- Ranero, C. R., Villaseñor, A., Phipps Morgan, J., Weinrebe, W., Relationship between bend-faulting at trenches and intermediate-depth seismicity, *Geochem. Geophys. Geosyst.*, 6, Q12002, doi:10.1029/2005GC000997, 2005.
- 925 Ranero, C. R., Grevemeyer, I., Sahling, H., Barckhausen, U., Hensen, C., Wallmann, K., Weinrebe, W., Vannucchi, P., von Huene, R., McIntosh, K., Hydrogeological system of erosional convergent margins and its influence on tectonics and interplate seismogenesis. *Geochemistry, Geophysics, Geosystems*, 9, Q03S04. <https://doi.org/10.1029/2007GC001679>, 2008.
- Richards, J.P., Jourdan, F., Creaser, R.A., Maldonado, G., DuFrane, S.A., Geology, geochemistry, geochronology, and economic potential of Neogene volcanic rocks in the Laguna Pedernal and Salar de Aguas Calientes segments of the Archibarca
- 930 lineament, northwest Argentina. *Journal of Volcanology and Geothermal Research* 258, 47–73, 2013.
- Rivera, O., Geodynamic Setting for Porphyry Copper Deposits in Central Chile: Role of Translithospheric Structures and Gravimetric Anomalies in Andean Metallogeny. Master Thesis, Department of Geological Sciences, Faculty of Engineering and Geological Sciences. Catholic University of the North, Chile 215 pp, 2017.
- Rivera, O., Cembrano, J., Modelo de Formación de Cuencas Volcano-Tectónicas en Zonas de Transferencia Oblicuas a la
- 935 Cadena Andina: El Caso de las Cuencas Oligo-Miocenas de Chile Central y su Relación con Estructuras WNW-NW (33°00' – 34°30' LS). In: 9º Congreso Geológico Chileno, Actas, vol. Nº2, p. 631-636, Puerto Varas, 2000.
- Roquer, T., Arancibia, G., Rowland, J., Iturrieta, P., Morata, D., Cembrano, J., Fault-controlled development of shallow hydrothermal systems: structural and mineralogical insights from the Southern Andes. *Geothermics* 66, 156-173, <http://dx.doi.org/10.1016/j.geothermics.2016.12.003>, 2017.
- 940 Roland, E., McGuire, J.J., Earthquake swarms on transform faults. *Geophysical Journal International*, 178: 1677-1690. <https://doi.org/10.1111/j.1365-246X.2009.04214.x>, 2009.
- Ruegg, J.C., Campos, J., Armijo, R., Barrientos, S., Briole, P., Thiele, R., et al., The Mw = 8.1 Antofagasta earthquake of July 30 1995: first results from teleseismic and geodetic data. *Geophys. Res. Lett.* 23 (9), 917–920, 1996.
- Ruiz, S., Madariaga, R., Historical and recent large megathrust earthquakes in Chile. *Tectonophysics*.
- 945 <http://dx.doi.org/10.1016/j.tecto.2018.01.015>, 2018.
- Ruiz, S., Madariaga, R., Astroza, M., Saragoni, G.R., Lancieri, M., Vigny, C., Campos, J., Short Period Rupture Process of the 2010 Mw 8.8 Maule Earthquake in Chile. *Earthquake Spectra*, Vol 28, N.S1, S1-S18, 2012.
- Ruiz, S., Metois, M., Fuenzalida, A., Ruiz, J., Leyton, F., Grandin, R., Vigny, C., Madariaga R., Campos, J. Intense foreshocks and a slow slip event preceded the 2014 Iquique Mw 8.1 earthquake. *Science*, 345, 1165-1169, DOI: 10.1126/science.1256074,
- 950 2014.
- Ruepke, L., Morgan, J., Hort, M., Connolly, J., Serpentine and the subduction water cycle. *Earth and Planetary Science Letters*. 223. 17-34. [10.1016/j.epsl.2004.04.018](https://doi.org/10.1016/j.epsl.2004.04.018), 2004.
- Salfity, J. A., Lineamentos transversales al rumbo andino en el Noroeste Argentino. In: IV Congreso Geológico Chileno, Antofagasta, Chile, Vol. 2, pp. 119–137, 1985..
- 955 Saffer, D.M., Tobin, H., Hydrogeology and Mechanics of Subduction Zone Forearcs: Fluid Flow and Pore Pressure. *Annu. Rev. Earth Planet. Sci.* 39. 157-186. [10.1146/annurev-earth-040610-133408](https://doi.org/10.1146/annurev-earth-040610-133408), 2011.

- Safer, D. M., Mapping fluids to subduction megathrust locking and slip behavior: Fluids and Subduction Megathrust Locking, *Geophys Res Lett* 44, 9337–9340, 2017.
- Sagripanti, L., Folguera, A., Gimenez, M., Rojas Vera, E.A., Fabiano, J.J., Molnar, N., Fennell, L., Ramos, V.A., Geometry of Middle to Late Triassic extensional deformation pattern in the Cordillera del Viento (Southern Central Andes): a combined field and geophysical study. *J. Iber. Geol.* 40, 349-366, 2014.
- Saillard, M., Audin, L., Rousset, B., Avouac, J.P., Chlieh, M., Hall, S.R., Husson, L., Farber, D.L., From the seismic cycle to long-term deformation: linking seismic coupling and Quaternary coastal geomorphology along the Andean megathrust, *Tectonics*, 36, doi:10.1002/2016TC004156, 2017.
- Sandwell, D. T., Müller, R. D., Smith, W. H., Garcia, E., & Francis, R., New global marine gravity model from CryoSat-2 and Jason-1 reveals buried tectonic structure. *Science*, 346(6205), 65-67, 2014.
- Santibáñez I., Cembrano, J., García-Pérez, T., Costa, C., Yáñez, G., Marquardt, C., Arancibia, G., González, G., Crustal faults in the Chilean Andes: geological constraints and seismic potential, *Andean Geology*, 46 (1): 32-65. Doi: 10.5027/andgeoV46n1-3067, 2019.
- Satake, K., Heidarzadeh, M., A Review of Source Models of the 2015 Illapel, Chile Earthquake and Insights from Tsunami Data. In: Braitenberg, C., Rabinovich, A. (eds) *The Chile-2015 (Illapel) Earthquake and Tsunami*. Pageoph Topical Volumes. Birkhäuser, Cham. https://doi.org/10.1007/978-3-319-57822-4_1. 2017.
- Scholz, C. H., *The Mechanics of Earthquakes and Faulting* (2nd Edition), Cambridge University Press, 504p, 1990.
- Scholz, C. H., Campos, J., The seismic coupling of subduction zones revisited, *J. Geophys. Res.*, 117, B05310, doi:10.1029/2011JB009003, 2012.
- Schurr, B., Asch, G., Rosenau, M., Wang R., Oncken, O., Barrientos, S., Salazar, P., Vilotte, J.P., The 2007M7.7 Tocopilla northern Chile earthquake sequence: Implications for along-strike and downdip rupture segmentation and megathrust frictional behavior, *J. Geophys. Res.*, 117, B05305, doi:10.1029/2011JB009030, 2012.
- Schurr, B., Asch, G., Hainzl, S., et al., Gradual unlocking of plate boundary controlled initiation of the 2014 Iquique earthquake. *Nature* 512, 299–302 <https://doi.org/10.1038/nature13681>, 2014
- SERNAGEOMIN, Mapa Geológico de Chile 1:1.000.000: digital version. Servicio Nacional de Geología y Minería, Digital Geological Publication No. 4 (CD-ROM, version 1.0). Santiago, Chile, 2003.
- Shillington, D., Bécel, A., Nedimović, M., et al., Link between plate fabric, hydration and subduction zone seismicity in Alaska. *Nature Geosci* 8, 961–964. <https://doi.org/10.1038/ngeo2586>, 2015.
- Sibson, R.H., Conditions for fault-valve behavior, in Knipe, R.J., and Rutter, E.H., eds., *Deformation Mechanisms, Rheology and Tectonics: Geological Society [London] Special Publication 54*, p. 15–28, <https://doi.org/10.1144/GSL.SP.1990.054.01.02>, 1990.
- Sibson, R.H., . Preparation zones for large crustal earthquakes consequent on fault-valve action. *Earth, Planets and Space* 72:31, <https://doi.org/10.1186/s40623-020-01153-x>, 2020.

- 990 Sielfeld, G., Lange D., Cembrano, J., Intra-Arc Crustal Seismicity: Seismotectonic Implications for the Southern Andes Volcanic Zone, Chile. *Tectonics* 38, 552–578, <https://doi.org/10.1029/2018TC004985>, 2019.
- Stanton-Yonge, A., Griffith, W.A., Cembrano, J., St. Julien, R., Iturrieta, P., Tectonic role of margin-parallel and margin-transverse faults during oblique subduction in the Southern Volcanic Zone of the Andes: Insights from boundary element modelling: *Tectonics* 35, 1990–2013, <https://doi.org/10.1002/2016TC004226>, 2016.
- 995 Talwani P., *Intraplate Earthquakes*, Cambridge University press, 360p, 2014.
- Thingbaijam K. K. S., Mai, P.M., Goda, K., New Empirical Earthquake Source-Scaling Laws. *Bulletin of the Seismological Society of America*; 107 (5): 2225–2246. Doi: <https://doi.org/10.1785/0120170017>, 2017.
- Torres, J., Caracterización del lineamiento Laguna fea-volcán san Pedro, región del Maule: Relación con actividad magmática e hidrotermal. Undergraduate thesis. Valdivia: Universidad Austral de Chile, 174, 2021.
- 1000 Tsuji, T., Ashi, J., Ikeda, Y., Strike-slip motion of a mega-splay fault system in the Nankai oblique subduction zone. *Earth Planet Sp* 66, 120. <https://doi.org/10.1186/1880-5981-66-120>, 2014.
- Vigny, C., Socquet, A., Peyrat, S., Ruegg, J.C., Métois, M., Madariaga, R., et al., The 2010 Mw 8.8 Maule Megathrust Earthquake of Central Chile, Monitored by GPS, *Science*, 1417-1421, 332, 6036, American Association for the Advancement of Science, doi: 10.1126/science.1204132, 2011.
- 1005 Wall, R., Gana, P., Gutiérrez, A., Mapa Geológico del Área de San Antonio- Melipilla. Regiones de Valparaíso, Metropolitana y del Libertador Bernardo O'Higgins. Mapas Geológicos N°2, Escala 1:100.000. Sernageomin, Chile, 1996..
- Wall, R., Sellés, D., Gana, P., Geología del Área Tiltil-Santiago, Región Metropolitana de Santiago. Serie Mapas Geológicos N°11, Escala 1:100.000. Sernageomin, Chile, 1999.
- Wallace, L. M., Beavan, J., McCaffrey, R., & Darby, D., Subduction zone coupling and tectonic block rotations in the North Island, New Zealand. *Journal of Geophysical Research*, **109**, B12406. <https://doi.org/10.1029/2004JB003241>, 2004.
- 1010 Wang, K., Bilek, S.L., Do subducting seamounts generate or stop large earthquakes? *Geology* 39, 819–822.
- Wdowinski, S., (1992). Dynamically supported trench topography, *J. Geophys. Res.*, 97(B12), 17651– 17656, doi:10.1029/92JB01337, 2011.
- Wiemer, D., Hagemann, S.G., Hayward, N., Begg, G.C., Hronsky, J., Thébaud, N., Kemp, A.I.S., Villanes, C., Cryptic trans-
- 1015 lithospheric fault systems at the western margin of South America: implications for the formation and localization of gold-rich deposit superclusters. *Frontiers in Earth Science* 11, 1159430, doi: 10.3389/feart.2023.1159430, 2023.
- Xia, S., Sun J., Huang, H., Degree of serpentinization in the forearc mantle wedge of Kyushu subduction zone: quantitative evaluations from seismic velocity. *Marine Geophysical Research*, 36, 101-112, 2015.
- Yáñez-Cuadra, V., Ortega-Culaciati, F., Moreno, M., Tassara, A., KrummNualart, N., Ruiz, J., et al,
- 1020 Interplate coupling and seismic potential in the Atacama Seismic Gap (Chile): Dismissing a rigid Andean sliver. *Geophysical Research Letters*, 49, e2022GL098257. <https://doi.org/10.1029/2022GL098257>, 2022.
- Yañez, G., Gana, P., Fernández, R., Sobre el origen y significado geológico de la anomalía Melipilla, zona central de Chile. *Revista Geológica de Chile*, 25, No. 2, 175-198, 1998.

- 1025 Yañez, G., Ranero, C.R., Von Huene, R., Díaz, J., Magnetic anomaly interpretation across the southern central Andes (32°-34°S): The role of the Juan Fernandez Ridge in the late Tertiary evolution of the margin. *Journal of Geophysical Research*, 106, 6325-6345, 2001.
- Yañez, G., Cembrano, J., The role of the viscous plate coupling in the late tertiary Andean deformation. *Journal of Geophysical Research*, vol 106, 6325-6345, 2004.
- 1030 Yañez, G., Rivera, O., Crustal dense blocks in the fore-arc and arc region of Chilean ranges and their role in the magma ascent and composition. *Breaking paradigms in the Andean metallogeny*, *Journal of South American Earth Sciences*, 93, pp. 51-66. DOI: 10.1016/j.jsames.2019.04.006, 2019.
- Yue, L.T., Brodsky, E., An, C., The 1 April 2014 Iquique, Chile, Mw 8.1 earthquake rupture sequence, *Geophys. Res. Lett.*, 41, 3818– 3825, doi:10.1002/2014GL060238, 2014.
- 1035 Zienkiewicz, O. C., Taylor, R.L., *The Finite Element Method*, vol. 2, *Solid and Fluid Mechanics Dynamics and Non-linearity*, 4th ed., McGraw-Hill, New York, 1991.